Stability and structure of a supercooled liquid mixture in two dimensions

Donna N. Perera[1,*] and Peter Harrowell[2,†]
[1]*Aperiodic Solids Research Team, National Research Institute for Metals (NRIM), 1-2-1 Sengen, Tsukuba, Ibaraki 305-0047, Japan*
[2]*School of Chemistry, University of Sydney, Sydney, New South Wales, 2006, Australia*
(Received 9 November 1998)

The structural and thermodynamic properties of a two-dimensional binary mixture of soft discs are reported over a range of temperatures down to large supercoolings using constant NPT molecular dynamics simulations. It is shown that the four orders of magnitude increase in the structural relaxation time is not accompanied by any significant increase in translational or orientational order. The phase diagram, calculated in the temperature/composition plane using thermodynamic integration, exhibits a deep eutectic point that is responsible for stabilizing the amorphous state. Voronoi analysis of the low-temperature ground state reveals a structure characterized by a network of linear arrays of fivefold and sevenfold sites. The heat capacity C_P exhibits an asymmetric peak with a maximum at $T^*=0.55$. It is argued that the initial rapid drop in C_P for $T^*<0.55$ is an equilibrium result and, hence, the peak in the heat capacity corresponds to the existence of an ''enthalpy gap'' with a characteristic temperature of $T^*\approx 0.35$. This gap results from a minimum volume change associated with an anharmonic fluctuation. [S1063-651X(99)07705-3]

PACS number(s): 64.70.Pf, 61.20.Lc, 02.70.Ns, 61.20.Ja

I. INTRODUCTION

Of all the puzzling features of glass-forming liquids, it is the presence of mechanical stability without order that represents the core problem. It is straightforward, after all, to understand why particle configurations of high symmetry, such as found in crystals, should correspond to potential energy minima (or, at least, extrema) and hence represent rigid states [1]. Rigid amorphous configurations, on the other hand, typically provide no such simple clues as to why they have been ''selected'' from the huge space of possible configurations for the special status of stability. The presence of these noncrystalline minima is the origin of the roughness of the potential energy surface over the space of configurations and, in a general sense, the slow dynamics at low temperature. Their existence also fuels the speculation concerning ''hidden'' phase transitions, on cooling, into some low energy subset of these stable structures.

In this paper we explore the nature of stability, mechanical and thermodynamical, in a two-dimensional (2D) glass-forming liquid through molecular dynamics (MD) simulations. The system is a binary mixture of discs interacting via a soft $1/r^{12}$ repulsion with a diameter ratio of 1.4. Elsewhere [2], we present a study of the relaxation dynamics and its spatial distribution in the same 2D liquid. The particle size ratio has been chosen so as to maximize disruption of crystal structures while avoiding liquid-liquid separation. A 2D model has been selected for simulation speed and, more importantly, the relative ease with which collective motions can be analyzed. As the role of dimensionality on the glass transition is currently an open question, we begin our report with an analysis of what is required of a *bone fide* glass-forming liquid and the degree to which the 2D mixture meets these criteria. This is followed by an identification of the thermodynamically stable phases, the properties of the amorphous ground state and the nature of the low temperature fluctuations out of this state. We are unaware of any previous simulation study of a glass-forming liquid that has included parallel studies of the relaxation dynamics and the thermodynamics of the model.

The binary mixture in 2D has, over recent years, become a popular model system for studying collective behavior in supercooled liquids. Deng, Argon, and Yip [3–6] have examined the topological features of a supercooled mixture of Lennard-Jones particles in 2D via MD simulations. In addition to characterizing the distribution of local environments, these workers also studied the kinetics of the structure during aging and shear flow. Muranaka and Hiwatari [7] have published MD results on the same softcore mixture as used in this paper. They observed large regions of highly correlated particle trajectories occurring on the same time scale as the β relaxation and proposed that such motions were the origin of the fast secondary relaxation. Nonequilibrium MD simulations of this same system have been carried out by Yamamoto and Onuki [8], who studied the dynamics of the equimolar mixture at equilibrium and under shear. They reported an increase in the characteristic length scale of the distribution of ''fast'' particles with decreasing temperature. The effect of an applied shear flow on these dynamic heterogeneities was found to be similar to that of an increase in the temperature. These workers have also established a qualitative similarity between the glassy phenomenology in 2D and 3D mixture models. Mel'cuk *et al.* [9] have also presented MD results of the existence of long-lived clusters, characterized by crystal-like environments, near the glass transition of a 2D binary mixture of Lennard-Jones (LJ) particles. Finally, Sadr-Lahijany *et al.* [10] have examined the process of dispersion-induced disordering in a 2D system, first examined by Bocquet and co-workers [11]. In this MD study, a phase diagram is presented in the space of density and the dispersion in the size of the Lennard-Jones discs. A critical

*Electronic address: dperera@tamamori.nrim.go.jp
†Author to whom correspondence should be addressed. Electronic address: peter@chem.usyd.edu.au

dispersion is associated with a continuous phase transition between crystal and liquid.

The literature on glassy alloys is extensive. The propensity of a mixture to sidestep crystallization is typically found to be enhanced in the vicinity of the maximal freezing point depression afforded by a eutectic point. Such features are commonly attributed to interaction potentials that favor the association of unlike species and hence resist the segregation necessary for crystallization [12]. In this paper we shall provide evidence of a deep eutectic in a binary alloy in the absence of *any* attractive interactions.

The paper is arranged as follows. Following the description of computational details in Sec. II, we shall demonstrate the slowing down of structural relaxation on cooling of the mixture and examine the various types of structural correlations for signs of long-range order in Sec. III. Next, we examine the relative stability of the amorphous phase to pure crystals of each component through the fate of heterogeneous simulations. In Sec. IV, we determine the equation of state for the mixture and calculate the chemical potential difference between liquid and ordered crystals. The object of this section is twofold, to establish at what point the liquid mixture should be regarded as a metastable state, and to try and understand the origin of the stability of this disordered state. In Sec. V, we study the amorphous phase: the temperature dependence of its extensive properties, its topological structure, the properties of its ground state, and the nature of its elementary fluctuations through the heat capacity and thermal expansivity.

II. MODEL AND COMPUTATIONAL DETAILS

The 2D system consists of an equimolar mixture of two types of particles with diameters $\sigma_2=1.4$ and $\sigma_1=1$, respectively, but with the same mass m. The three pairwise additive interactions are given by the purely repulsive softcore potentials

$$u_{ab}(r)=\epsilon\left[\frac{\sigma_{ab}}{r}\right]^{12}, \quad a,b=1,2, \tag{1}$$

where $\sigma_{aa}=\sigma_a$ and $\sigma_{ab}=(\sigma_a+\sigma_b)/2$. The cutoff radii of the interactions are set at $4.5\sigma_{ab}$. The units of mass, length, and time are m, σ_1, and $\tau=\sigma_1\sqrt{m/\epsilon}$, respectively.

A total of $N=1024$ particles were enclosed in a square box with periodic boundary conditions. The simulations were carried out at constant number of particles, pressure ($P^*=P\sigma_1^2/\epsilon$) and temperature ($T^*=k_BT/\epsilon$, where k_B is Boltzmann's constant), using the constraint MD algorithm of Evans and Morriss [13,14]. In this method, the instantaneous temperature and pressure are strict constants of the motion. The system is initially driven to the desired temperature by velocity scaling and to the desired pressure by the use of a Newton-Raphson convergence scheme. A third-order (four-value) Gear predictor-corrector algorithm was used to integrate the equations of motion [14]. The time step employed was 0.0025τ for $T^*>1$, and 0.005τ for $T^*\leqslant 1$. In argon units of $\epsilon=120k_B$, $m=6.6\times10^{-23}$ g, and $\sigma_1=3.4$ Å, these time steps correspond to approximately 5 and 10 fs, respectively.

The pressure was fixed at $P^*=13.5$ and temperatures in the range $T^*\in[0.1,5]$ were studied. The freezing temperature of the single component system of small particles at this pressure is $T^*_{f,1}=0.95$, and the corresponding temperature for the large particles is $T^*_{f,2}=1.7$. The starting configuration of the run at $T^*=5$ was a square lattice of alternating large and small particles whereas, for each of the lower temperatures, the initial configuration for the equilibration run came from the final configuration of the preceding higher temperature run. For $T^*\geqslant 0.4$, the equilibration times were longer than the times taken for all the dynamic correlation functions investigated to decay to zero. Below $T^*=0.4$, however, the system is no longer able to reach equilibrium within the finite time scale of the experiment. For these low temperatures, the equilibration run was taken out until steady state was achieved, i.e., when the average thermodynamic properties remained constant. Table I lists the equilibration and production times.

III. IS THE 2D BINARY MIXTURE A GLASS FORMER?

Experimentally, finding an amorphous configuration which is unable to relax on the observational time scales is a nontrivial result. The same cannot be said, however, for simulations of liquids where it is trivial to reduce the observation time to the point where relaxation is not possible. Criteria are needed, therefore, to distinguish a metastable liquid capable of forming a glass from an unstable one which has simply not been observed long enough to detect the ordering transition. In this paper, we apply the following two criteria.

(i) A glass-forming liquid must exhibit relaxation times which grow rapidly on cooling without the development of long-range correlations associated with established ordered phases.

(ii) In a glass-forming liquid, the disordered or amorphous state must represent a stationary state in the sense that it is stable over time scales at least an order of magnitude longer than the relaxation time for fluctuations within that state.

Few would argue with the first criterion. We note that this criterion implies that ''disordered'' or ''amorphous'' (we shall treat these as equivalent terms) includes *all* forms of order minus the restricted set of ''established'' ordered phases. The second criterion is necessary if we are to be able to speak about reproducible amorphous states. There are certainly phenomena, such as aging and nonlinear response to temperature jumps, which call for the study of nonstationary states. Such problems are not precluded by criterion (ii) which simply allows us to establish whether a nonstationary state is relaxing to an amorphous state (as defined by our criteria) or towards an ordered one. The distinction is as crucial for these nonstationary problems as for those involving linear responses. A state which satisfies criterion (ii) will be referred to as being at equilibrium. While *metastable* equilibrium is more accurate, it is unwieldy and, given our failure to observe any hint of crystallization in the equimolar mixture, unnecessary. As we shall demonstrate, the properties of the supercooled mixtures exhibit a smooth continuation from the true equilibrium liquid at high temperatures. We shall now consider the 2D binary mixture in the light of criteria (i) and (ii).

TABLE I. The thermodynamic averages and their root mean square (rms) deviations for all temperatures investigated for the equimolar binary mixture with $\sigma_2/\sigma_1=1.4$. Also shown are the effective coupling constant Γ_e defined in Eq. (4), the compressibility factor $Z=P^*/(\rho^*T^*)$, the equilibration time t_{eqlb}, and the production time t_{run} for each of these states.

T^*	t_{eqlb}/τ	t_{run}/τ	U^*	E^*	H^*	ρ^*
5	846	375	3.0753	8.0753	31.527	0.57567
3	1443	375	3.0503	6.0503	27.353	0.63375
2	2040	375	3.0250	5.0250	25.175	0.66997
1	2040	2050	2.9830	3.9830	22.881	0.71435
0.9	2040	2050	2.9775	3.9775	22.642	0.71943
0.8	2040	2050	2.9716	3.7716	22.401	0.72466
0.7	2040	2050	2.9659	3.6659	22.161	0.72991
0.6	4510	8100	2.9599	3.5599	21.919	0.73532
0.55	6060	8100	2.9567	3.5067	21.797	0.73808
0.5	7142	9100	2.9523	3.4523	21.666	0.74118
0.46	23235	9100	2.9502	3.4102	21.571	0.74334
0.4	52515	25010	2.9459	3.3459	21.421	0.74687
0.35	17000	22050	2.9435	3.2935	21.303	0.74958
0.3	10000	20500	2.9430	3.2430	21.205	0.75162
0.2	10000	20500	2.9422	3.1422	20.996	0.75615
0.1	10000	20500	2.9418	3.0418	20.792	0.76054

T^*	Γ_e	Z	rms(U^*)	rms(E^*)	rms(H^*)	rms(ρ^*)
5	0.65164	4.6902	0.0223	0.0223	0.156	0.00329
3	0.78102	7.1006	0.0141	0.0141	0.098	0.00252
2	0.88338	10.075	0.0097	0.0097	0.068	0.00194
1	1.0572	18.898	0.0052	0.0052	0.036	0.00117
0.9	1.0836	20.850	0.0048	0.0048	0.034	0.00110
0.8	1.1131	23.287	0.0042	0.0042	0.029	0.00098
0.7	1.1464	26.422	0.0037	0.0037	0.026	0.00088
0.6	1.1850	30.599	0.0032	0.0032	0.022	0.00076
0.55	1.2068	33.256	0.0029	0.0029	0.021	0.00071
0.5	1.2313	36.428	0.0027	0.0027	0.019	0.00064
0.46	1.2521	39.481	0.0024	0.0024	0.017	0.00060
0.4	1.2877	45.189	0.0021	0.0021	0.014	0.00051
0.35	1.3215	51.457	0.0017	0.0017	0.012	0.00042
0.3	1.3596	59.871	0.0014	0.0014	0.0098	0.00035
0.2	1.4634	89.268	0.00092	0.00092	0.0064	0.00023
0.1	1.6522	177.51	0.00045	0.00045	0.0032	0.00012

A. Incoherent scattering functions

It is straightforward to establish the rapid growth of the time scales on cooling. In Fig. 1, we present the set of incoherent scattering functions

$$F_{s,a}(k,t)=\frac{1}{N_a}\left\langle \sum_{j=1}^{N_a} \exp\{i\mathbf{k}\cdot[\mathbf{r}_j(t)-\mathbf{r}_j(0)]\}\right\rangle, \quad a=1,2, \tag{2}$$

for both particle species. The angular brackets denote an average over time origins and an angular average over the directions of the wave vector $\mathbf{k}$. The magnitude of $\mathbf{k}$ was chosen to be $k_1=7.17\sigma_1^{-1}$ for $F_{s,1}(k,t)$ and $k_2=5.60\sigma_1^{-1}$ for

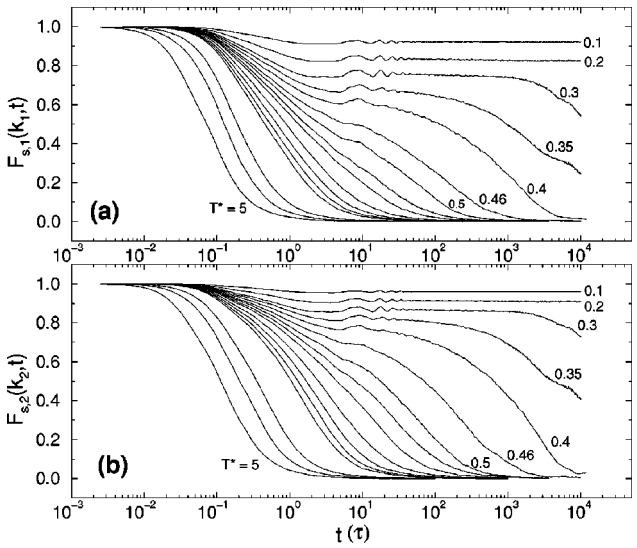

FIG. 1. Incoherent scattering functions (a) $F_{s,1}(k_1,t)$ and (b) $F_{s,2}(k_2,t)$ for the small and large particles, respectively. The wave vectors $k_1=7.17\sigma_1^{-1}$ and $k_2=5.60\sigma_1^{-1}$ are the first peak positions in the respective partial structure factors. From left to right, the relaxation curves correspond to the following temperatures: $T^*=5$, 3, 2, 1, 0.9, 0.8, 0.7, 0.6, 0.55, 0.5, 0.46, 0.4, 0.35, 0.3, 0.2, and 0.1. Observe the appearance of a slower relaxation process at $T^*=0.5$.

$F_{s,2}(k,t)$. These correspond to the positions of the first peak maximums in the respective partial structure factors, which are only weakly dependent on temperature. Figure 1 demonstrates that the scattering functions are able to decay to zero for $T^*\geqslant 0.4$. Below this temperature, structural relaxation cannot fully proceed to equilibrium due to the finite time scale of the simulations. We draw attention to the two-step decay process of the relaxation functions at the lower temperatures. The step is first observed at $T^*\approx 0.5$. Elsewhere [2,15,16] we examine the changes in dynamics associated with this crossover. As the temperature is lowered further we

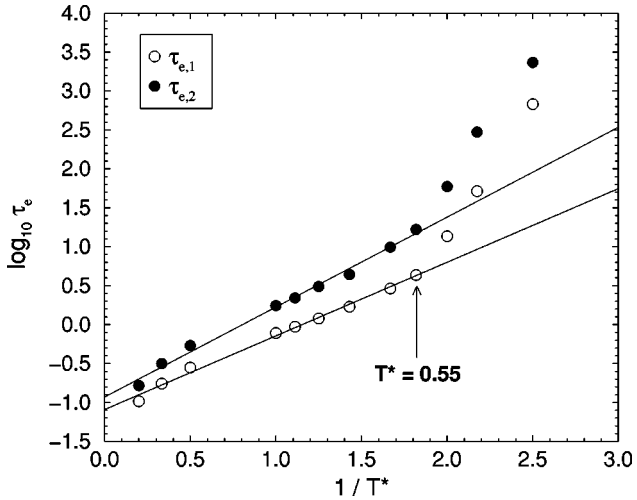

FIG. 2. A log-linear plot of the structural relaxation times $\tau_{e,1}$ and $\tau_{e,2}$, as defined in the text, against $1/T^*$ for the small and large particles respectively. Note the positive deviation from Arrhenius behavior for $T^*<0.55$. The solid lines are linear regressions through the data points in the range $T^*\in[0.55,5]$.

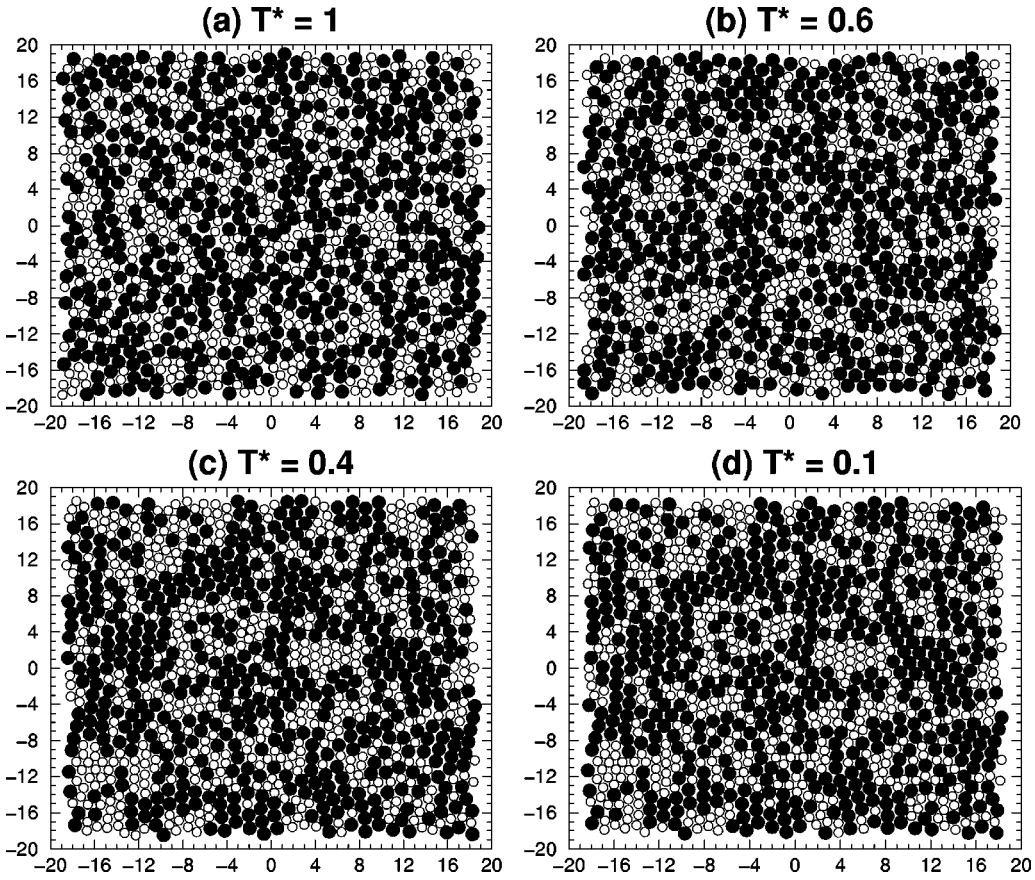

FIG. 3. Representative particle configurations at (a) $T^*=1$, (b) $T^*=0.6$, (c) $T^*=0.4$, and (d) $T^*=0.1$ for the equimolar binary mixture with $\sigma_2/\sigma_1=1.4$. The small and large particles are represented by the open and filled circles respectively and have been drawn slightly smaller than their actual sizes to avoid significant overlapping that would obscure the pictures.

see the plateau height increase. A structural relaxation time $\tau_{e,a}$ is defined as the time required for the incoherent scattering funtion $F_{s,a}(k,t)$ to equal $1/e$. Relaxation times for large and small particles are plotted against $1/T^*$ in Fig. 2. We find a rapid non-Arrhenius increase in $\tau_{e,1}$ and $\tau_{e,2}$ on cooling, in accord with the first part of criteria (i). A more comprehensive analysis of the dynamics of the 2D mixture is provided elsewhere [2].

B. Structural correlations

Is the slowing down associated with the appearance of some form of long-range order? In the single component 2D liquid, for example, we find a significant slowing down on approaching the freezing transition as a result of the steadily growing domains of hexagonal order [17]. Comparison of particle configurations in the mixture at $T^*=0.1$, 0.4, 0.6, and 1.0 in Fig. 3 certainly indicates an increasing tendency of the large particles to collect into hexagonal domains. In what follows, we examine translational, compositional, and hexatic order in the equimolar mixture.

1. Partial pair distribution functions

For the 2D equimolar binary mixture with $\sigma_2/\sigma_1=1.4$, we find no long-range translational order. The partial pair distribution functions $g_{ab}(r)$ decay exponentially, as shown in Figs. 4–6, even at the lowest temperatures. The splitting of the second peak which we observe in all three $g_{ab}(r)$'s can be simply accounted for by the presence of the two particle sizes in the mixture. Details of this analysis are provided in Ref. [18]. Appearing, as this feature does, at a temperature ($T^*\approx 1.0$) well above any glasslike behavior, we conclude that it has nothing to do with the glass transition. A similar conclusion with respect to a 3D binary mixture of Lennard-Jones particles has been reached by Bernu *et al.* [19] and Kob and Andersen [20].

The partial distribution functions are also sensitive measures of local compositional correlations. Integrating under the first peak of the distribution functions out to the first minimum, provides the partial coordination numbers $n_{ab}(1)$ which are plotted against T^* in Fig. 7(a). In decreasing the temperature from $T^*=0.5$ to $T^*=0.4$, we observe a small step increase in $n_{11}(1)$ and $n_{22}(1)$, from approximately 2.6 to 2.9 and approximately 3.6 to 3.8, respectively, which is accompanied by a corresponding drop in $n_{12}(1)$. This change represents a slight increase in the tendency to microsegregation and clear evidence of the absence of global demixing. The step is more pronounced in the second shell coordination numbers $n_{ab}(2)$ as shown in Fig. 7(b). We stress that these distribution functions were found to be stable over the long run times indicated in Table I. At $T^*=0.4$, for example, the total run time corresponds to ≈ 50 times the structural relaxation time $\tau_{e,1}$. We will consider the stability of the low-temperature disordered states further below. The stationary character of the local distributions, however, is one of the

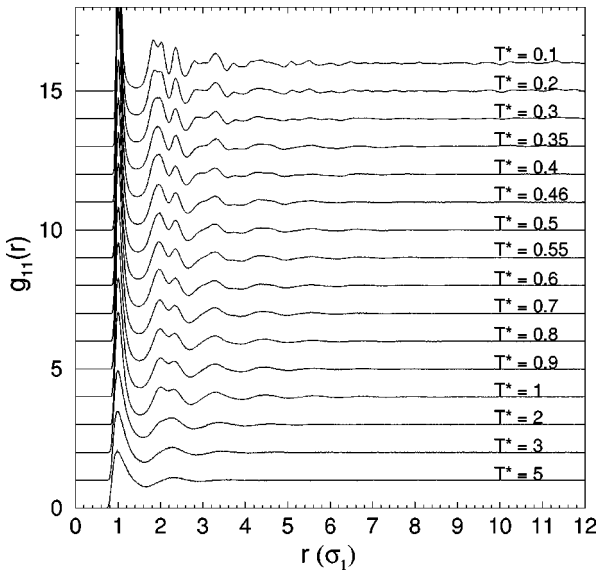

FIG. 4. The partial pair distribution function $g_{11}(r)$ as a function of distance from $T^*=5$ down to $T^*=0.1$ for the equimolar binary mixture with $\sigma_2/\sigma_1=1.4$. The pair distribution functions have been constructed with a spatial resolution of $0.01\sigma_1$. For $T^*\leqslant 3$, each curve has been shifted upwards by one unit from the higher temperature curve directly preceding it.

strongest pieces of evidence that the amorphous liquids represent stationary states.

2. Partial structure factors

The mechanical stability of a liquid with respect to the development of periodic order can be best defined in terms of its susceptibility to a perturbing field with a wavelength **k**. In the case of a binary mixture, the Fourier amplitude $\delta\hat{\rho}_a(\mathbf{k})$ of the resulting perturbation in the density of component a

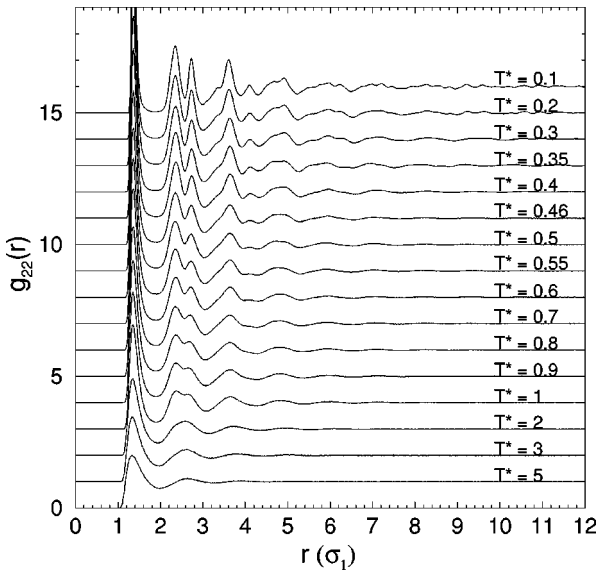

FIG. 5. The partial pair distribution function $g_{22}(r)$ as a function of distance from $T^*=5$ down to $T^*=0.1$ for the equimolar binary mixture with $\sigma_2/\sigma_1=1.4$. For $T^*\leqslant 3$, each curve has been shifted upwards by one unit from the higher temperature curve directly preceding it.

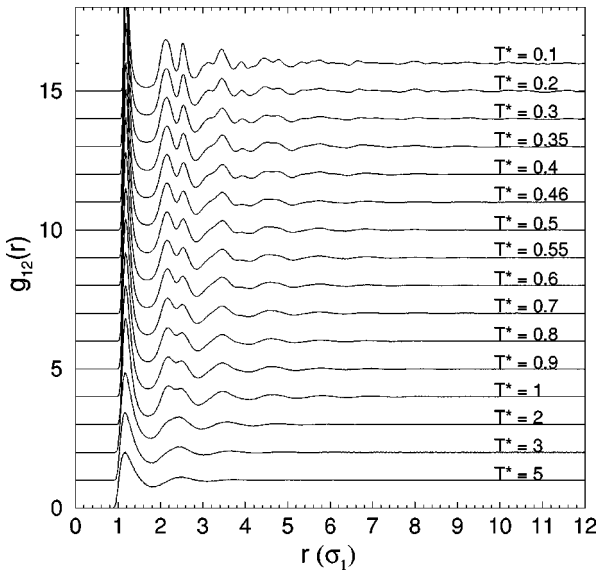

FIG. 6. The partial pair distribution function $g_{12}(r)$ as a function of distance from $T^*=5$ down to $T^*=0.1$ for the equimolar binary mixture with $\sigma_2/\sigma_1=1.4$. For $T^*\leqslant 3$, each curve has been shifted upwards by one unit from the higher temperature curve directly preceding it.

due to the action of a perturbing field with Fourier amplitude $\delta\hat{\phi}_b(\mathbf{k})$ acting on component b is given by

$$\delta\hat{\rho}_a(\mathbf{k})=\chi_{ab}(\mathbf{k})\,\delta\hat{\phi}_b(\mathbf{k}). \tag{3}$$

The susceptibilities $\chi_{ab}(\mathbf{k})=-(\rho_a/k_BT)S_{ab}(\mathbf{k})$. The partial structure factors are calculated as follows [21]:

$$S_{ab}(k)=x_{ab}\delta_{ab}+x_ax_b\rho^*\hat{h}_{ab}(k), \quad a,b=1,2, \tag{4}$$

where $\hat{h}_{ab}(k)$ is the Fourier transform of the total correlation function $h_{ab}(r)=g_{ab}(r)-1$. The Fourier transformations of $g_{ab}(r)$ were carried out using Filon's method [22]. If an instability is present, it will be identified by the divergence of the appropriate partial structure factors.

In Figs. 8 and 9 we plot $S_{11}(k)$ and $S_{22}(k)$ for all temperatures investigated. The curves have been displaced vertically for clarity. The oscillations at small k below the first maxima are artifacts of the Fourier transformation procedure and should be ignored. In both partial structure factors, the position of the first maximum is only very weakly dependent on temperature. For $S_{22}(k)$, the second peak is also split into two components at low temperatures, unlike the case for $S_{11}(k)$. The components of the bimodal second peak in $S_{22}(k)$ occur at wave vectors which coincide with the second and third peaks at $k\approx 9.2\sigma_1^{-1}$ and $k\approx 10.5\sigma_1^{-1}$, respectively, in the static structure factor of a *single* component crystal of large particles. We conclude that this feature is due to the presence of crystalline domains of large particles at low temperatures.

Klein and co-workers [9,23] have proposed (i) that supercooled liquids can exhibit a spinodal instability with respect to the crystalline phase and (ii) that such an instability is responsible for a rigid amorphous phase. To examine the behavior of the susceptibilities at low temperatures we plot, in Fig. 10, the height of the first peak of $S_{11}(k)$ and $S_{22}(k)$

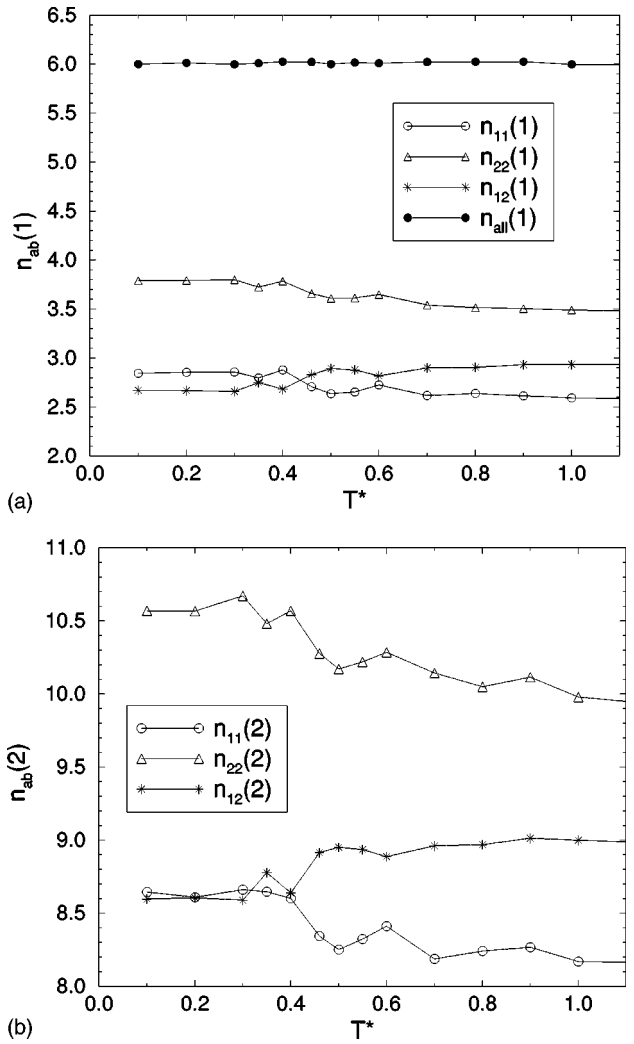

FIG. 7. (a) The temperature dependence in the range $T^* \leqslant 1$ of the first shell partial coordination numbers $n_{11}(1)$, $n_{22}(1)$, and $n_{12}(1)$, calculated up to the position of the first minimum in $g_{11}(r)$, $g_{22}(r)$, and $g_{12}(r)$, respectively, for the equimolar binary mixture with $\sigma_2/\sigma_1 = 1.4$. Also shown is the temperature dependence of the average number of first nearest neighbors irrespective of particle type $n_{all}(1)$, calculated by integrating up to the position of the first minimum in the total radial distribution function $g(r) = x_1^2 g_{11}(r) + 2x_1 x_2 g_{12}(r) + x_2^2 g_{22}(r)$. Observe that the average number of first nearest neighbors is 6 for $T^* \leqslant 1$. (b) The temperature dependence in the range $T^* \leqslant 1$ of the partial coordination numbers $n_{11}(2)$, $n_{22}(2)$, and $n_{12}(2)$, calculated by integrating $g_{11}(r)$, $g_{22}(r)$, and $g_{12}(r)$, respectively, out to the *second* minimum in each case. Note the distinct increase in the clustering of like species in going from $T^* = 0.5$ to $T^* = 0.4$ and the corresponding drop in $n_{12}(2)$.

against temperature. The temperature dependence of these peaks $S_{aa}(\max)$ can be reasonably described by a power law of the form $S_{aa}(\max) \propto T^{*-\gamma_{aa}}$ (with $\gamma_{11} = 0.08$ and $\gamma_{22} = 0.16$) for $T^* \geqslant 0.4$. This extrapolation places any instability at $T^* = 0.0$. The breakdown of these power laws at low temperatures, however, must raise doubts about the validity of such an extrapolation. The observed stability of the amorphous phase implies a ''cap'' on the magnitude of the structure factor peaks, leaving higher values of $S_{11}(\max)$, $S_{12}(\max)$, and $S_{22}(\max)$ simply inaccessible to the supercooled liquid. This underlying stability of the amorphous

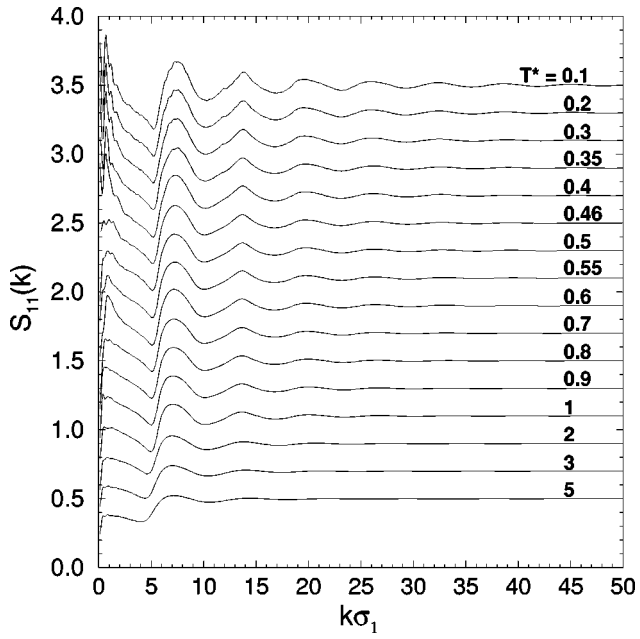

FIG. 8. Partial structure factor $S_{11}(k)$ for all temperatures investigated for the equimolar binary mixture with $\sigma_2/\sigma_1 = 1.4$. For clarity, each curve below $T^* = 5$ has been displaced vertically by 0.2 units above the higher temperature curve directly preceding it.

phase, evident only at low temperatures, would seem to render any spinodal inferred from fits to higher-temperature structure factors as physically irrelevant. Standard linear response theory has the rate of structural relaxation proportional to the corresponding susceptibility. The observed increase in $S_{22}(k)$, for example, at the first peak therefore can account for only a 1.5-fold increase in $\tau_{e,2}$, as opposed to the observed increase of roughly 4.5 orders of magnitude over the temperature range $0.4 \leqslant T^* \leqslant 5.0$. We shall return to the idea of cluster instabilities in Sec. V E. We conclude that (i)

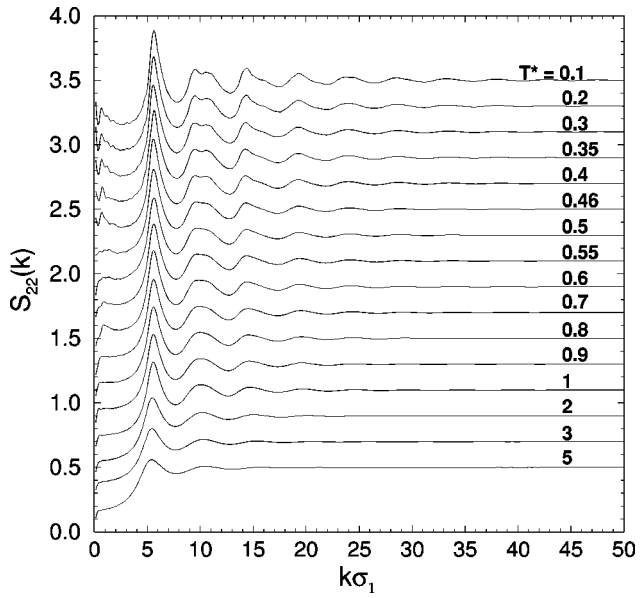

FIG. 9. Partial structure factor $S_{22}(k)$ for all temperatures investigated for the equimolar binary mixture with $\sigma_2/\sigma_1 = 1.4$. For clarity, each curve below $T^* = 5$ has been displaced vertically by 0.2 units above the higher temperature curve directly preceding it.

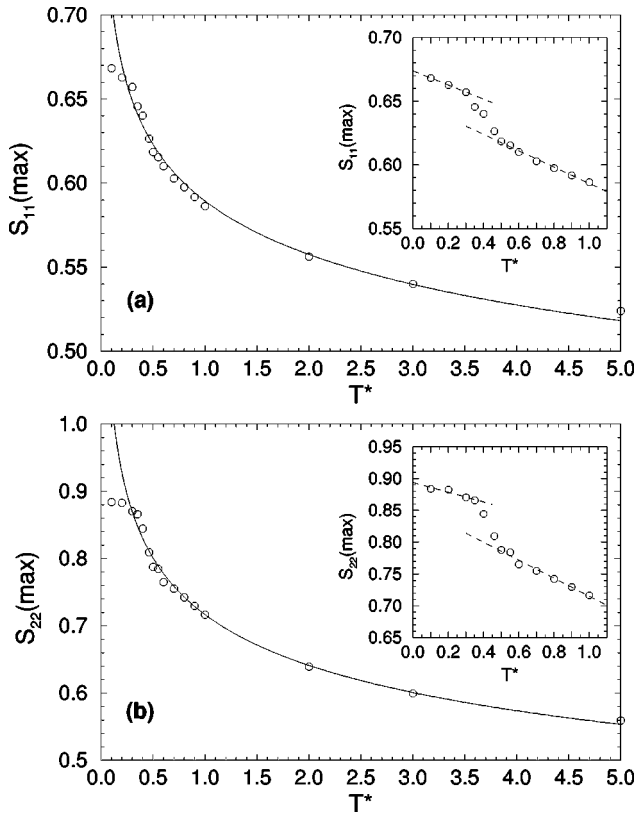

FIG. 10. The temperature dependence of the heights of the first peak, (a) $S_{11}(\max)$ and (b) $S_{22}(\max)$, in the partial structure factors $S_{11}(k)$ and $S_{22}(k)$, respectively. The solid lines are power law fits of the forms (a) $S_{11}(\max)=0.5892T^{*-0.07995}$ and (b) $S_{22}(\max)=0.7164T^{*-0.1604}$. The insets show the peak heights for $T^*\leqslant 1$. Observe the steplike increase in the peak heights below $T^*=0.5$. The dashed lines are linear regressions through the MD data points in the temperature intervals $0.1\leqslant T^*\leqslant 0.3$ and $0.5\leqslant T^*\leqslant 1$.

the observed slowing down is not the result of the development of long-range translational order and (ii) the increase local structure is insufficient to account for the increasing relaxation time without a physical picture of the *kinetic* correlations between structurally uncorrelated regions.

3. Orientational order and its spatial correlation

Having established the absence of long-range translational order in the 2D mixture down to temperatures of $T^*=0.1$, we must also test for long-range orientational correlation of the local hexagonal domains. The existence of a hexatic phase in the one component soft disc liquid, lying between the liquid and the crystal, has been established in simulations of large systems ($N>16\,000$) over a very narrow range of densities [24]. The effect on this transition by quenched disorder is a topic of considerable current interest, particularly due to its connection with the ordering of flux lines in high T_c superconductors. Nelson [25] has suggested that such disorder would suppress the freezing temperature to a greater extent than the liquid-hexatic transition, thereby expanding the range of the orientationally ordered phase. Above a certain critical amount of disorder, the crystal would not form. In the case where disorder arises from a distribution of particles sizes, a recent 2D simulation [10] identifies a critical size dispersity (roughly density independent), above which ordered phases are unstable.

We shall return to the question of phase transitions in the 2D mixture (see Sec. V E). Our prime interest here is simply to establish whether our low-temperature mixture exhibits local hexagonal order and the spatial correlations of the orientation of this order. Following Broughton and co-workers [27], an orientational order parameter $\Psi(\mathbf{r}_j)$ is defined for the jth particle

$$\Psi(\mathbf{r}_j)=\frac{1}{n_j}\sum_{k=1}^{n_j} e^{i6\Theta_{jk}} \tag{5}$$

where Θ_{jk} is the angle (in radians) made by the bond between particle j and particle k (one of j's n_j nearest neighbors), and an arbitrary direction (here chosen to be the x axis). For computational efficiency, the number of nearest neighbors was determined using a cutoff distance taken at the first minimum in the total radial distribution function for each temperature. The order parameter equals one if particle j lies at the center of a perfect hexagon made up of its neighbors. We shall define a set of bulk averaged hexagonal order parameters as follows:

$$\Psi=\left\langle \frac{1}{N}\sum_{j=1}^{N} |\Psi(\mathbf{r}_j)| \right\rangle \tag{6}$$

and

$$\Psi_a=\left\langle \frac{1}{N_a}\sum_{j=1}^{N_a} |\Psi(\mathbf{r}_j)| \right\rangle \quad \text{with } a=1,2. \tag{7}$$

The angular brackets denote an average over various configurations separated in time. These order parameters measure the average degree of local hexagonal order in the mixture. The spatial correlation of the orientation of these hexagonal environments is measured by the associated correlation functions

$$C(r)=\left\langle \frac{1}{N\rho^*}\sum_{j=1}^{N}\sum_{k\neq j}^{N} \Psi(\mathbf{r}_j)\Psi^*(\mathbf{r}_k)\,\delta(r-|\mathbf{r}_j-\mathbf{r}_k|) \right\rangle \tag{8}$$

and

$$C_a(r)=\left\langle \frac{1}{N\rho^* x_a^2}\sum_{j=1}^{N_a}\sum_{k\neq j}^{N_a} \Psi(\mathbf{r}_j)\Psi^*(\mathbf{r}_k) \times \delta(r-|\mathbf{r}_j-\mathbf{r}_k|) \right\rangle, \quad a=1,2. \tag{9}$$

In Fig. 11 we present the values of the average bulk order parameters Ψ, Ψ_1, and Ψ_2 over the range of temperatures studied. For comparison, we have included the analogous order parameter for a single component liquid of soft discs with diameter σ_1. We note the following features: (1) A significant amount of local hexagonal order is present even in high-temperature liquids. For $T^*>1.0$ single and binary mixtures have similar amounts of local order, despite the structural incompatability of the two components in the mixture. This is the result of a degree of microsegregation in the mixture which allows for relatively unimpeded local order-

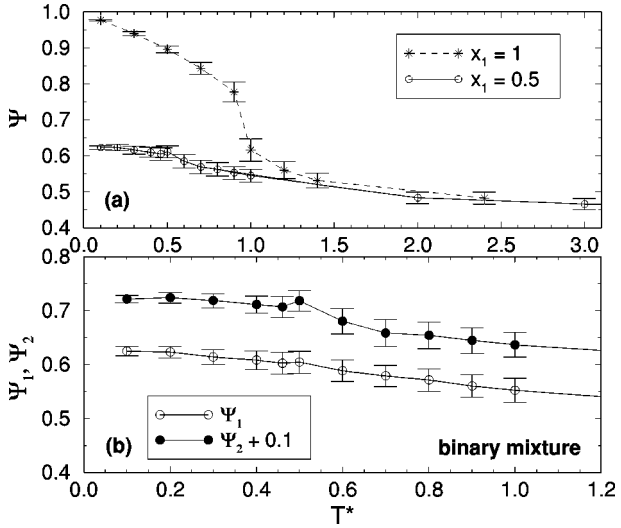

FIG. 11. (a) The temperature dependence of the bulk averaged hexagonal order parameter Ψ as defined in Eq. (6) for the equimolar ($x_1=0.5$) binary mixture with $\sigma_2/\sigma_1=1.4$ and for the monocomponent system of small particles ($x_1=1$). (b) The temperature dependence in the range $T^*\leqslant 1$ of the small (Ψ_1) and large (Ψ_2) particle contributions to the hexagonal order parameter Ψ of the equimolar binary mixture shown in (a). Ψ_2 has been shifted upwards by 0.1 units for clarity. The results in (a) and (b) have been averaged over 1000 equally spaced configurations along the production run for each temperature. The error bars are twice the standard deviation about the average.

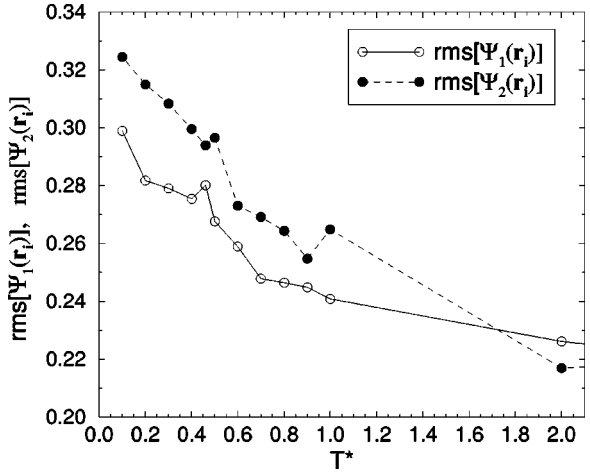

FIG. 12. The temperature dependence of the root mean square (rms) deviations of the local hexagonal order parameters $\Psi_1(\mathbf{r}_j)$ and $\Psi_2(\mathbf{r}_j)$ for the equimolar binary mixture.

ing. (2) As the one component liquid orders on cooling, the mixture order parameter increases slowly and steadily in a smooth continuation of the high-temperature behavior. (3) At $0.5<T^*<0.6$, we see a small step in Ψ_2 corresponding to a slight increase in structure among the large particles. This temperature coincides, roughly, with that predicted to be the freezing point in the mixture (see Sec. IV B). (4) As $T^*\rightarrow 0$, the hexagonal order in the amorphous mixture approaches 65% of that of the zero-temperature single component crystal.

While the average local order parameters only increase gradually on cooling, it is possible that there might be a more abrupt increase in the order of *individual* domains, offset in the bulk averaging by regions of low order. This would show up as an abrupt increase in the width of the distribution of the *local* order parameters on cooling. To test this idea we have plotted the temperature dependence of the root mean square deviation $\sqrt{\langle[\Psi_a(\mathbf{r}_j)-\langle\Psi_a(\mathbf{r}_j)\rangle]^2\rangle}$ of the local hexagonal order parameter for $a=1$ and 2 in Fig. 12. We find only a continuous increase in the width of the distributions on cooling, with no sign of any sudden increase in the bimodal character of the structural distribution.

The hexatic correlation functions $C(r)$, $C_1(r)$, and $C_2(r)$ provide an explicit measure of the spatial extent of the orientational correlation between local hexagonal environments as measured by the analogous hexatic order parameter. The orientational correlation functions defined in Eqs. (8) and (9) are weighted by the translational correlations. To see the orientational correlations free of this bias, we have plotted the ratios $C(r)/g(r)$, $C_1(r)/g_{11}(r)$, and $C_2(r)/g_{22}(r)$ over a range of temperatures in Figs. 13, 14, and 15, respectively. In the mixtures we find that all hexatic correlation functions remain shortranged over the entire temperature range studied. While reminding the reader that, for $T^*<0.4$ these values do not correspond to equilibrium results, we can conclude that the structural arrest observed in our simulations does not arise from the appearance of any observable form of long-range order.

The absence of long-range orientational order at low temperatures presents a picture different from that described by Mel'cuk *et al.* [9]. Reference [9] reports the presence of crystalline clusters whose size increases with cooling in a binary mixture of Lennard-Jones discs. The key difference in the two methods of analyzing extended structure is that the approach of Ref. [9] includes clusters made up of orientationally uncorrelated domains of hexagonal order.

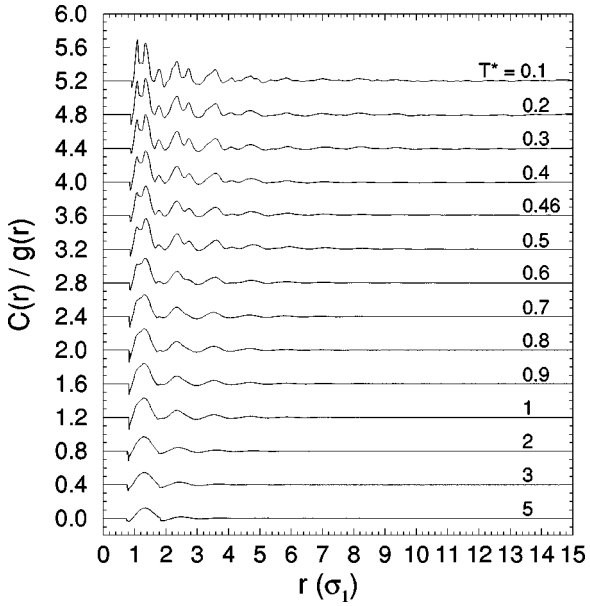

FIG. 13. The orientational correlation function $C(r)/g(r)$, as defined in the text, calculated for $0.1\leqslant T^*\leqslant 5.0$. For very short distances less than interparticle separations, the function is undefined and has been set equal to zero. For clarity, functions have been offset vertically by 0.4 units above the preceding curve.

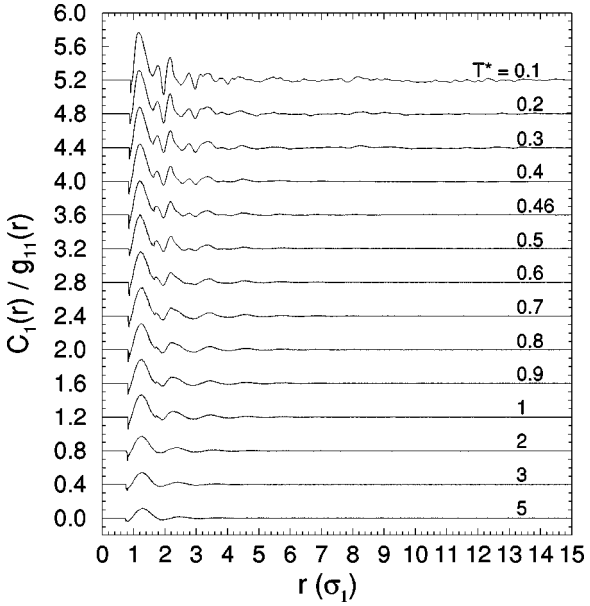

FIG. 14. The partial orientational correlation function $C_1(r)/g_{11}(r)$ for the small particles, as defined in the text, calculated for $0.1 \leqslant T^* \leqslant 5.0$. For clarity, functions have been offset vertically.

C. The fate of crystal+crystal configurations

To conclude this examination of the 2D binary mixture's glass-forming credentials, we consider here the stability of the amorphous state. For $T^* \geqslant 0.4$ we find the disordered state to show no sign of ordering or demixing over time intervals in excess of $10\tau_{e,a}$. No sign of either instability has been observed at any temperature. To try and separate thermodynamic from kinetic stability in the amorphous state, we have carried out a series of runs over a range of temperatures which start from slabs of the two pure crystals in contact.

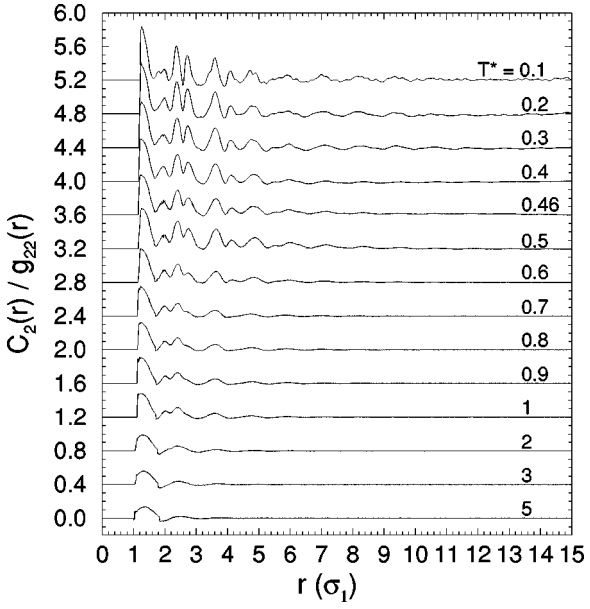

FIG. 15. The partial orientational correlation function $C_2(r)/g_{22}(r)$ for the large particles, as defined in the text, calculated for $0.1 \leqslant T^* \leqslant 5.0$. For clarity, functions have been offset vertically.

Spontaneous melting and mixing provides a clear indication of thermodynamic stability of the amorphous state. Snapshots of the time evolution of a representative run at $T^* = 0.7$ are shown in Fig. 16. The initial configuration, with velocities taken from a disordered liquid at the same temperature, began with a high pressure $P^* \approx 15.7$ for the $T^* = 0.7$ run. The initial several hundred time steps of the run, therefore, involve the mechanical equilibration of the pressure to $P^* = 13.5$. As can be seen in Fig. 16, the crystalline configurations are eventually disrupted. The resulting amorphous state appears identical, in terms of the average structural parameters and thermodynamical properties, to that obtained by a quench to the same temperature from the high temperature liquid. We find complete recovery of the amorphous state for $T^* \geqslant 0.6$. This melting and mixing is remarkable. Well below the freezing points of either crystal, we have spontaneous melting driven solely by the entropy of mixing. Work is done by this mixing as the density of the system drops with the disordering by $\approx 2\%$ of the initial density.

For $T^* \leqslant 0.5$, we observe no disordering of any kind from the crystal-crystal simulations. This change in behavior is quite distinct. Despite the long time required for the large particle crystal to dissolve completely at $T^* = 0.7$, permeation of some of the particles of both species across the intercrystal boundaries is already observed for times less than 10000τ. This is also true for a lower temperature of $T^* = 0.6$. However, at $T^* = 0.5$, the particles of the two crystalline phases in contact showed no tendency to move across the interphase and to penetrate the solid phase of the other, even on time scales about two orders of magnitude longer than the time taken for the incoherent and intermediate scattering functions of the disordered mixture at this temperature to decay to zero (see Fig. 1). The simulation run was stopped at $t = 56\,000\tau$ for $T^* = 0.5$ due to this absence of any sign of mixing between the two particle species.

Clearly, for $T^* \geqslant 0.6$ the liquid state is thermodynamically stable. The change in behavior at $T^* = 0.5$ could be due to a rapid increase in relaxation times of the crystal with respect to the relaxation time of the amorphous phase at this temperature, or to the crystals becoming thermodynamically stable. To see if we could observe crystal growth at $T^* = 0.5$ we stopped a melting run at $T^* = 0.7$ half way through and quenched it down to $T^* = 0.5$. The remaining ''chunk'' of large particle crystal showed no signs of growing or melting despite the run continuing for times 3 orders of magnitude longer than the appropriate structural relaxation time ($\tau_{e,2}$). We conclude that the kinetics of melting and freezing slow down more quickly than the structural relaxation of the ''equilibrated'' amorphous phase. This result means that, below $T^* = 0.6$, these heterogeneous simulations can no longer help us to identify the thermodynamically stable phase.

IV. INVESTIGATING THE PHASE DIAGRAM

A. Equation of state

One advantage of studying systems with inverse power potentials that has long been recognized is the inherent scaling of thermodynamic properties [28,29]. All the reduced excess static properties depend on two independent variables only, which are chosen to be the number concentration x_1

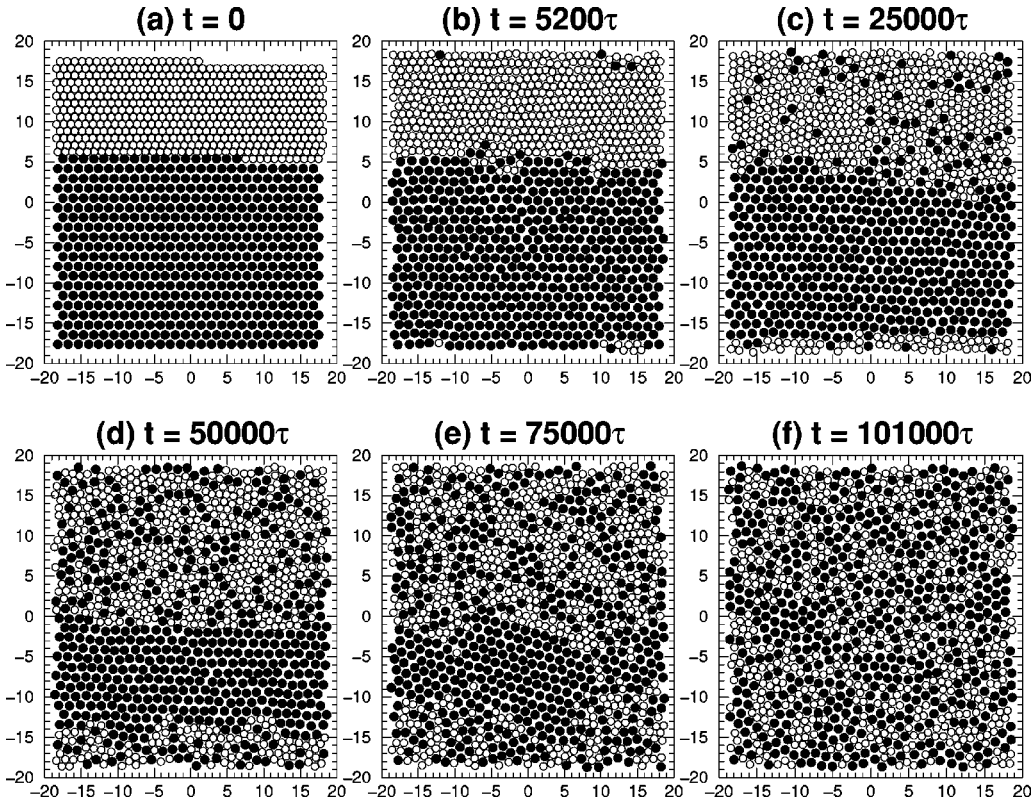

FIG. 16. Time evolution of a crystal-mixing simulation at $T^*=0.7$ and $P^*=13.5$ for the equimolar binary mixture with $\sigma_2/\sigma_1=1.4$. The small and large particles are represented by the open and filled circles, respectively. The discs are not drawn to scale.

$=N_1/N$ (where $N=N_1+N_2$ and $x_2=1-x_1$), and a composite density-temperature variable $\Gamma=\rho^*(T^*)^{-d/n}$, where d is the dimension of the system, n is the exponent in the potential, and $\rho^*=N\sigma_1^d/V_d$ is the reduced number density, with V_d the volume in d dimensions. The composite variable Γ is often referred to as a coupling constant. For the inverse twelfth power potential of Eq. (1) in 2D, Γ is given by

$$\Gamma=\rho^*(T^*)^{-1/6}, \tag{10}$$

where $\rho^*=N\sigma_1^2/A$ and A is the total area of the simulation box. In the treatment of binary mixtures of spherical particles, the equation of state of the mixture can be approximated quite well by an effective one component system of particles with diameter σ_e [19,29]. The corresponding effective coupling constant for the 2D binary mixture is

$$\Gamma_e=\Gamma\left[\frac{\sigma_e}{\sigma_1}\right]^2. \tag{11}$$

We have chosen the effective diameter to be

$$\sigma_e^2=x_1\sigma_1^2+x_2\sigma_2^2, \tag{12}$$

instead of the more commonly used diameter

$$\sigma_e'^2=\sum_i\sum_j x_i x_j\sigma_{ij}^2 = x_1^2\sigma_1^2+2x_1x_2\sigma_{12}^2+x_2^2\sigma_2^2, \tag{13}$$

for reasons outlined below. For the equimolar binary mixture with $\sigma_2/\sigma_1=1.4$, $\sigma_e^2=1.48$, and $\sigma_e'^2=1.46$. Although this difference is small, the corresponding equations of state can differ significantly in the precision in which they are able to fit the MD results as described below.

From our MD data for the equimolar binary mixture in the range $T^*=0.4$ to 5 where equilibrium can be reached within the simulations, we fit an eighth degree polynomial to the compressibility factor $Z=P^*/(\rho^*T^*)$, as a function of Γ_e using the effective diameter σ_e in Eq. (12). The resulting polynomial is

$$Z_{p1}=1+1.77306\Gamma_e+2.36241\Gamma_e^2+2.10798\Gamma_e^3+7.69487\Gamma_e^4 -16.23890\Gamma_e^5+27.99087\Gamma_e^6-16.86430\Gamma_e^7 +5.46998\Gamma_e^8, \tag{14}$$

with the second and third coefficients being constrained to be the exact second and third virial coefficients of a single component 2D system with this potential, as given by Broughton, Gilmer, and Weeks [27]. If the effective diameter σ_e' of Eq. (13) is used instead, then the following polynomial, with the second and third coefficients constrained as before, is obtained:

$$Z_{p2}=1+1.77306\Gamma_e+2.36241\Gamma_e^2-4.34023\Gamma_e^3+26.92186\Gamma_e^4 -20.88440\Gamma_e^5-3.40501\Gamma_e^6+17.58996\Gamma_e^7 -4.94193\Gamma_e^8. \tag{15}$$

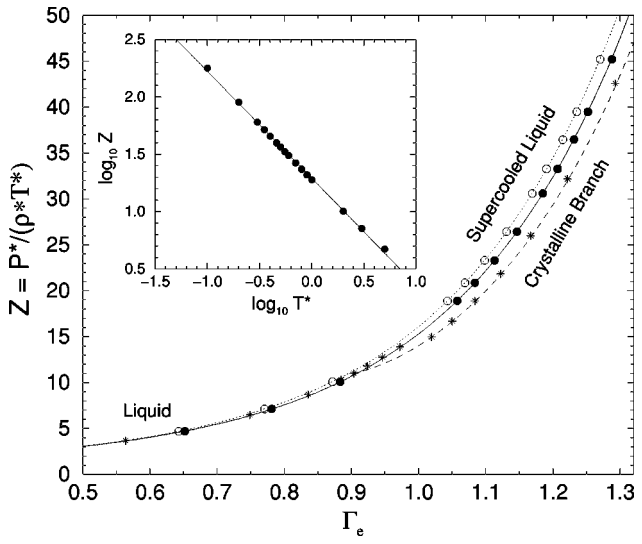

FIG. 17. The main figure shows our MD results for the compressibility factor $Z=P^*/(\rho^* T^*)$ of the equimolar binary mixture with $\sigma_2/\sigma_1=1.4$, as a function of Γ_e, where Γ_e is calculated using the effective diameter σ_e of Eq. (12) (solid circles) and σ_e' of Eq. (13) (open circles). These two sets of data are fitted using the polynomials Z_{p1} of Eq. (14) (solid line) and Z_{p2} of Eq. (15) (dotted line), respectively. Also shown are our simulation results for the monocomponent system of small particles $(x_1=1,\sigma_1=1)$ (asterisks). The equation of state for the crystalline branch of the pure liquid, as shown by the dashed line, is from Broughton *et al.* [27] and is given by Eq. (16). Note that for the pure system $\Gamma_e=\Gamma$. The inset shows that Z for the equimolar binary mixture can also be expressed as a simple power law $Z=AT^{*B}$ with $A=19.4178$ and $B=-0.9311$, as determined from the solid line which is a linear regression through all the data points.

In Fig. 17 is plotted our MD results for Z for the equimolar binary mixture as a function of Γ_e using σ_e (solid circles) and σ_e' (open circles), and the corresponding polynomial fits Z_{p1} (solid line) and Z_{p2} (dotted line). Also shown are our simulation results for the single component system of small particles $(x_1=1,\sigma_1=1)$ at the same pressure $P^*=13.5$. It can be seen that the MD results for the binary mixture using σ_e extend continuously below the freezing point of the single component system which occurs at $\Gamma_e=\Gamma=0.986$ as determined by Broughton and co-workers [27]. The polynomial Z_{p1} is able to fit the entire liquid branch of the single component system with a deviation of less than 2%. In fact, below $T^*=2$, as the freezing transition is approached, the accuracy of Z_{p1} in fitting the MD data of the monocomponent system increases, becoming better than 99.6% at $T^*=1$. With regards to the equimolar binary mixture, this polynomial Z_{p1} is able to fit the MD results down to $T^*=0.2$ with a deviation of less than 0.3%.

The second polynomial Z_{p2} fits the results of the single component liquid just as well as Z_{p1} at high temperatures. However, unlike Z_{p1}, for $T^*<2$, Z_{p2} tends to overestimate the compressibility factor with deviations greater than 2%, and appears to depart further away from the single component MD results as the freezing point is approached as shown in Fig. 17. For example, at $T^*=1$, Z_{p2} overestimates the compressibility factor of the monocomponent system by more than 4.5%. For this reason, we have chosen to use the effective diameter σ_e of Eq. (12) and to represent the equation of state of the entire liquid and amorphous branch of the effective one component system by the polynomial Z_{p1}. The success of Eq. (12) over Eq. (13) may reflect the local demixing which we find, particularly at low temperatures. The effective diameter of Eq. (13) corresponds to a random mixing approximation.

We find that the polynomial Z_{p1} is able to fit the full range of our simulated states for the equimolar mixture from $T^*=5$ $(\Gamma_e=0.6516)$ to $T^*=0.1$ $(\Gamma_e=1.6521)$. The continuous variation of this equation of state indicates that there is no phase transition, since such a transition would result in a departure from this continuous curve.

We have tested the effective one component approximation for other 2D binary mixtures with $\sigma_2=1.2$, 1.6, and 2, either as a function of composition at fixed temperature, or as a function of temperature at fixed composition, all at the same constant pressure of $P^*=13.5$ [18]. For the binary mixture of $\sigma_2=1.4$, we have also simulated states at a fixed temperature of $T^*=0.8$ for compositions ranging from $x_1=0$ to 0.9 in steps of 0.1. It is found that up to $\sigma_2/\sigma_1=1.6$, binary mixtures that are not too concentrated with the larger particles, i.e., not too close to $x_2=1$, seem to obey very well the effective one component equation of state given by Z_{p1}. However, for $x_2\rightarrow 1$, the compressibility factors for these diameter ratios tend to deviate away from the liquid curve and approach the crystalline branch. The effective one component approximation breaks down for $\sigma_2/\sigma_1=2$, even for a concentration of large particles as low as $x_2=0.1$ at $T^*=1$.

The equation of state for the single component crystal, as shown by the dashed line in Fig. 17, is a polynomial fit from Broughton and co-workers [27] expressed as

$$Z_s=7+7.60602\Gamma^6-1.24044\Gamma^{-6}+0.64663\Gamma^{-12}. \quad (16)$$

We find that this empirical function is able to fit our own simulation results for the monocomponent crystal (as shown by the asterisks in Fig. 17) with an accuracy of greater than 99%.

The freezing temperature of the single component system of small particles $(\sigma_1=1)$ at the constant pressure of $P^*=13.5$ has already been determined by Broughton *et al.* [26,27] to be $T^*_{f,1}=0.95$ which is why we have chosen to perform our simulations at this pressure. The state at $T^*_{f,1}$ corresponds to $\Gamma_1=0.986$ and a compressibility factor of $Z_1=14.493$. This agrees with our own simulation results which show a hysteresis region for the thermodynamic properties between $T^*\approx 0.94$ and 0.96. From the scaling properties of the softcore potential [Eqs. (10) and (11)], the freezing temperature of the monocomponent system of large particles $(\sigma_2=1.4)$ at the same pressure of $P^*=13.5$, where the unit of length is still constrained at $\sigma_1=1$, can be calculated by equating the compressibility factor of this system Z_2, to Z_1, and by setting $\Gamma_2=\Gamma(\sigma_2/\sigma_1)^2=\Gamma_1$ at the freezing point. The solution yields a freezing temperature of $T^*_{f,2}=1.70$ for the large particles, also in agreement with our simulation results.

B. The phase diagram

Following the procedure by Broughton *et al.* [27], the chemical potential of the binary mixture in the effective one component framework $\Delta\mu_{\rm eff}$ relative to that of the ideal gas and excluding the ideal mixing term is given by

$$\beta\Delta\mu_L=\int_0^{\Gamma_e}\left\{\frac{1}{\Gamma_e'}\frac{\partial[(Z_{p1}-1)\Gamma_e']}{\partial\Gamma_e'}\right\}d\Gamma_e', \tag{17}$$

where $\beta=1/(k_BT)$. Substituting Eq. (14) into the above and performing the integration gives

$$\begin{aligned}\beta\Delta\mu_{\rm eff}=&3.54612\Gamma_e+3.54361\Gamma_e^2+2.81064\Gamma_e^3+9.61859\Gamma_e^4\\&-19.48668\Gamma_e^5+32.65601\Gamma_e^6-19.27348\Gamma_e^7\\&+6.15373\Gamma_e^8.\end{aligned} \tag{18}$$

In order to calculate the chemical potential relative to that of the ideal gas for the individual components in the liquid mixture, $\Delta\mu_{La}$ where $a=1,2$, we assume that, since the equation of state Z_{p1} for the effective one component system fits the temperature dependence of the compressibility factor for the binary mixture with $\sigma_2/\sigma_1=1.4$ very well, the Gibbs free energy G_L of this mixture can be written as

$$\begin{aligned}G_L(N_1,N_2,T^*,P^*)=&G_{\rm eff}(N,T^*,P_{\rm eff}^*)\\&+\beta^{-1}(x_1\ln x_1+x_2\ln x_2),\end{aligned} \tag{19}$$

where $G_{\rm eff}$ is the free energy of the effective one component liquid and $P_{\rm eff}^*=P^*(\sigma_e/\sigma_1)^2$ is the reduced pressure for this effective liquid in units of σ_e^2/ϵ. The chemical potential of the small particles in the liquid mixture is then given by

$$\begin{aligned}\beta\Delta\mu_{L1}=&\beta\frac{\partial G_L}{\partial N_1}\\=&\beta\frac{\partial G_{\rm eff}}{\partial N}\bigg|_{T^*,P_{\rm eff}^*}\frac{\partial N}{\partial N_1}+\beta\frac{\partial G_{\rm eff}}{\partial P_{\rm eff}^*}\bigg|_{N,T^*}\frac{\partial P_{\rm eff}^*}{\partial N_1}+\ln x_1\\=&\beta\Delta\mu_{\rm eff}+\beta V^*P^*x_2\left(\frac{\sigma_1^2-\sigma_2^2}{\sigma_e^2}\right)+\ln x_1\\=&\beta\Delta\mu_{\rm eff}+Zx_2\left(\frac{\sigma_1^2-\sigma_2^2}{\sigma_e^2}\right)+\ln x_1,\end{aligned} \tag{20}$$

where $\partial G_{\rm eff}/\partial P_{\rm eff}^*|_{N,T^*}=V_{\rm eff}^*=V^*(\sigma_1/\sigma_e)^2$ and V^* is the area of the simulation box in units of σ_1^2. Similarly, the chemical potential for the large particles in the mixture is given by

$$\beta\Delta\mu_{L2}=\beta\Delta\mu_{\rm eff}+Zx_1\left(\frac{\sigma_2^2-\sigma_1^2}{\sigma_e^2}\right)+\ln x_2. \tag{21}$$

To construct the phase diagram, we must first decide upon the composition and structure of the crystal phases. We have chosen to use single component hexagonal crystals for both ordered phases. Our reasons are as follows. Substitutionally disordered crystals with the large particles as the minority component are extremely unlikely for any significant concentration of the large particles due to the choice of particle sizes. This, of course, was the very purpose of choosing the ratio 1:1.4. As a consequence, we choose a single component hexagonal crystal as the small particle-rich ordered phase.

The ordered phase in the large particle-rich part of the phase diagram offers more possibilities. Our simulations suggest that number ratios up to 0.1 of small particles might be accommodated within a substitutionally disordered hexagonal crystal of large particles. Xu and Baus [31], using a density functional (DF) theory, have found that a binary alloy of hard discs with a diameter ratio of 1.176 can freeze into a substitutionally disordered crystal with no sign of a eutectic phase. We have found a similar result in simulations of the soft disc mixture with a diameter ratio of 1.2. (This result, we note, is in contradiction to the recent calculations of Wheatley [32].) Deng *et al.* [3] also observe a freezing transition in an equimolar mixture with a diameter ratio of 1.244. They find that a supercooled liquid can be obtained with a sufficiently fast temperature quench.

With no other calculations of crystal free energies in 2D mixtures with a glass-forming diameter ratio, we turn to data on spheres for some indication of the ordered large particle-rich phase in a glass-forming mixture. The phase diagrams of binary hard sphere mixtures have been determined by Kranendonk and Frenkel [33] via Monte Carlo simulations for diameter ratios in the range $1\leqslant\sigma_2/\sigma_1\leqslant1.176$. As soft sphere mixtures with a diameter ratio of 1.2 *do* appear to form glasses [34,35], the phase diagram for the diameter ratio of 1.176 for the spheres is relevant. The ordered phases in the 1.176 system [33] are substitutionally disordered crystals which extend over compositional ranges of 10 and <5 % in the minority species for the large and small-rich regions, respectively. Using a DF theory, Denton and Ashcroft [36] have investigated the relative stabilities of various crystalline structures in coexistence with the equimolar composition of binary hard sphere mixtures for large size ratios. They conclude that for $\sigma_2/\sigma_1>1.31$ the miscibility gap between the small and large spheres becomes so great that a mechanically stable substituted solid is no longer possible and that the most stable structure is the single component face centered cubic crystal. Taking these results, along with our own, into consideration, we conclude that a substitutionally disordered crystal is probably stable for small concentrations of small particles. As the solubility of small particles in the large particle crystal is expected to be small, however, we believe that the pure hexagonal crystal of large particles will provide a reasonable approximation of the coexistence temperature for crystal and liquid mixture. The coexistence lines calculated using the pure crystals can be considered as lower bounds on the correct value. If more stable two component crystals exist, these will freeze at higher temperatures.

For the single component crystal, the chemical potential relative to that of the ideal gas and corresponding to the equation of state Z_s in Eq. (16), is derived by Broughton *et al.* [27] to be

$$\begin{aligned}\beta\Delta\mu_{S1}=&9.9105+6\ln\Gamma+8.87369\Gamma^6-1.03370\Gamma^{-6}\\&+0.592744\Gamma^{-12},\end{aligned} \tag{22}$$

where Γ is defined in Eq. (10). The corresponding expression

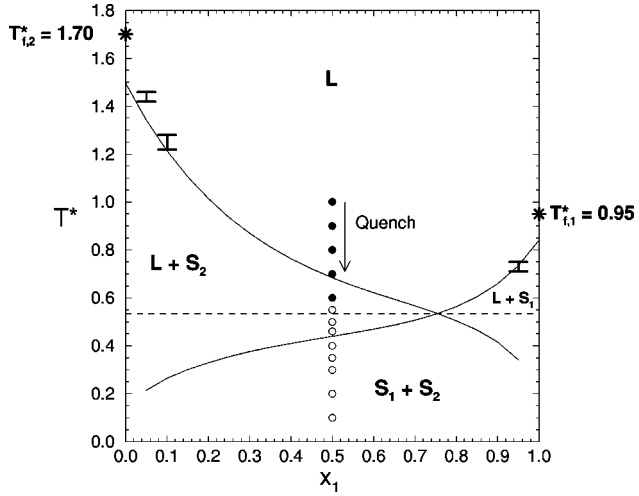

FIG. 18. The approximate phase diagram for the binary soft disc mixture with $\sigma_2/\sigma_1=1.4$ for a fixed pressure of $P^*=13.5$. The symbols **L**, $\mathbf{S}_1$, and $\mathbf{S}_2$ represent the liquid mixture, and the small and large particle crystals, respectively. The freezing temperatures of the single component systems $T^*_{f,1}$ and $T^*_{f,2}$, are shown by the asterisks. The solid lines are the coexistence curves calculated using Eqs. (20) to (22) by assuming that only one or the other of the monocomponent solids is in equilibrium with the liquid mixture at the coexistence temperatures. The eutectic point is given by the intersection of the two coexistence curves. It occurs at a composition of $x_1=0.75$ and a temperature of $T^*=0.54$. The error bars are the temperature intervals where a discontinuous change is observed in the temperature dependence of thermodynamic properties in the MD simulations at low solute concentrations. Also shown are the temperatures at which the simulated states of the quenched equimolar binary mixture for $T^*\leqslant 1$ are *thermodynamically* (solid circles) and *kinetically* (open circles) stable as determined from the crystal-mixing simulations described in Sec. III C.

for the chemical potential of the large particle crystalline phase $\beta\Delta\mu_{S2}$ is obtained by replacing Γ in the above equation with $\Gamma_2=\Gamma(\sigma_2/\sigma_1)^2$.

Thermodynamic equilibrium requires that $\beta\Delta\mu_{L1}=\beta\Delta\mu_{S1}$ along the coexistence line on the large x_1 side, and $\beta\Delta\mu_{L2}=\beta\Delta\mu_{S2}$ on the large x_2 side. The intersection of these two coexistence lines denotes the eutectic point for this phase diagram as shown in Fig. 18. The eutectic point occurs at $x_1\approx 0.75$ and $T^*\approx 0.54$. The presence of the eutectic is consistent with the hard disc mixture DF calculations of Xu and Baus [31] who observe a trend from spindle- to azeotrope- to eutectic-type phase diagrams as the diameter ratio increases. It is interesting that the hard sphere mixtures [33,36] show a similar trend in phases occurring at approximately the same diameter ratios. Recent simulations by Speedy [37] for the binary hard disc mixture with a diameter ratio of 1.4 suggest that this system also exhibits a eutectic.

The considerable depth of the eutectic, central to the stability of the glassy state, is something of a surprise in light of the almost continuous character of the one component freezing transition. The magnitude δ_e of the freezing point depression at the eutectic point can be defined in terms of the lower of the freezing points of the pure components (i.e., $T^*_{f,1}$, the freezing point of the small particles):

$$\delta_e=\frac{T^*_{f,1}-T^*_e}{T^*_{f,1}}, \tag{23}$$

where $T^*_e=0.54$ is the eutectic temperature. This depth, which is equal to 0.43, exceeds those of real binary alloy systems such as Ge-Sb ($\delta_e=0.061$), Ge-Zn ($\delta_e=0.061$), Ni-P ($\delta_e=0.093$), and Cd-Bi ($\delta_e=0.32$), but is shallower than the very deep Au-Si eutectic point ($\delta_e=0.66$) [38]. The presence of a deep eutectic in the 2D softcore mixture with purely *repulsive* interactions is particularly striking in light of the general consensus [39–42] that substantial freezing point depressions require large *attractive* interactions between *unlike* species, as is the case for the real binary alloys mentioned above. The explanation for the deep eutectics in the mixtures of purely repulsive particles (hard spheres show similarly large freezing point depressions [33]) may lie in the relatively small values of ΔH_f, the enthalpy of fusion, in these systems. For small concentrations X of solute, immiscible in the crystal phase of the major species, the freezing point depression is given by [43]

$$\delta T\approx(T_f^2/\Delta H_f)(1-X) \tag{24}$$

and a small value of ΔH_f will result in the entropy of mixing being dominant with a resulting large freezing point depression.

The mutual disruption of crystalline order which gives rise to the eutectic point also has consequences for the dynamics in the liquid phase in 2D, well above the eutectic temperature. We have observed [18,44] in simulations at $T^*=1.0$ that by adding large solute particles ($\sigma_2=1.4$) to the pure solvent of small particles, the self-diffusion constants of both the small and large particles increase, reaching a maximum at $x_1\approx 0.7$–0.8 and decreasing from then onwards as x_1 decreases. Enhanced diffusion at small solute concentrations has been directly linked [44] with the disruption of the local solvent structure about the larger solute particles. The decrease in the diffusion constants of both species at higher solute concentration is the result of solute clustering [18]. The coincidence of the composition at which the diffusion constants reach their maximum with that of the eutectic point are, we suggest, manifestations of the same local disruption of structure. We are unaware of any previous reports on a connection between solute enhanced dynamics and freezing point suppression.

At a composition of $x=0.5$, we predict that the large particles should freeze at $T^*=0.7$ (see Fig. 18), while we find in the simulations starting from the two pure crystals that both crystals melt at $T^*=0.6$. This difference could be accounted for as a consequence of the constraint of fixed numbers of particles. Coexistence at $T^*=0.7$ requires the large particle crystal to be in contact with an equimolar liquid mixture. The production of this mixture exhausts our supply of large particles. As we lower the temperature we also decrease the concentration of large particles needed in the liquid phase. The effect of the fixed values of N_1 and N_2 is to lower the actual transition temperature so that for $T^*\geqslant 0.6$ the liquid mixture is the equilibrium phase.

In the phase diagram of Fig. 18 we also show, by way of error bars, the temperature ranges at low solute concentrations corresponding to $x_1=0.05$, 0.1, and 0.95 where a discontinuous change is observed in the temperature dependence of average thermodynamic properties measured in our MD simulations. These results suggest a first-order phase

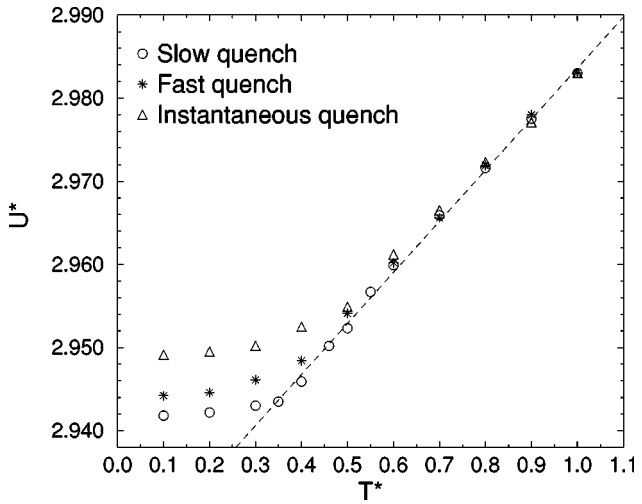

FIG. 19. The temperature dependence of the potential energy per particle U^* of the equimolar binary mixture ($\sigma_2/\sigma_1=1.4$) for three different cooling rates as described in Sec. V B. The MD data for the slow quench is also listed in Table I. The dashed line is a linear regression through the results for the slow quench in the temperature range $0.4\leqslant T^*\leqslant 1$ where the system is able to reach equilibrium.

transition from the dilute liquid mixture to a substitutionally disordered solid. A change in the temperature dependence of the thermodynamic properties is observed for $x_1>0.1$. As the number of small solute particles increase, we can no longer detect the abrupt changes in average density and potential energy which mark the freezing transition. As the concentration of small particles approaches 50% it seems reasonable to regard the polycrystalline character of the ground state obtained at $x_2=0.9$ as continuously transforming into the amorphous ground state in which the extent of any ordered domain is suppressed to a size similar to the liquid equilibrium correlation length.

V. PROPERTIES OF THE AMORPHOUS PHASE

A. Temperature dependence of the extensive properties

The thermodynamic averages for the potential energy per particle $U^*=U/(N\epsilon)$, energy per particle $E^*=E/(N\epsilon)$, enthalpy per particle $H^*=H/(N\epsilon)$, and number density ρ^*, are summarized in Table I for the range of temperatures investigated. Also tabulated are the compressibility factor Z, the effective coupling constant Γ_e defined in Eq. (11), as well as the root mean square (rms) deviations of the instantaneous thermodynamic properties from their averages, calculated as $\sqrt{\langle p^2\rangle-\langle p\rangle^2}$ where p is the property of interest and the angular brackets denote an average over time. The rms deviations are, of course, system-size dependent, increasing with decreasing number of particles. The results in Table I are for $N=1024$. We have also investigated a smaller system of $N=512$ and find that the average thermodynamic properties are equal to those of the larger system within statistical error.

The potential energy per particle U^* is plotted as open circles in Fig. 19 for $0.1\leqslant T^*\leqslant 1$. For $1<T^*\leqslant 5$, U^* increases with decreasing slope as T^* increases. However, within the temperature range $0.4\leqslant T^*\leqslant 1$, U^* varies approximately linearly with temperature. For $T^*\leqslant 0.3$, the average potential energy departs from the high temperature extrapolation as the system is no longer able to relax completely within the simulation run. This departure to a smaller slope at the very lowest temperatures is also mirrored in E^*, H^*, and ρ^*, and gives rise to rounded steps in the first order temperature derivatives of these properties as described later below. If the computer glass transition temperature T_g^* is defined to be the temperature at which the high- and low-temperature extrapolated lines intersect, then $T_g^*\simeq 0.35$. This change in slope of the thermodynamic averages in the vicinity of T_g^* is not, however, reflected in the compressibility factor Z which varies smoothly and continuously with Γ_e through this region as shown in Fig. 17. We have found that, within the range $0.1<T^*<5.0$, the compressibility factor can be approximated very well by a simple power law (see Fig. 17):

$$Z=AT^{*B}, \tag{25}$$

where $A=19.4178$ and $B=-0.9311$. This apparent continuity between liquid and glass has been questioned recently by Speedy [45] in a careful study of the hard sphere glass. Note that the power law above is slightly less accurate than the polynomial Z_{p1} of Eq. (14) in fitting the MD data for the binary mixture. The power law deviates from the MD results by less than 3% in the range $0.1<T^*<5$, whereas at $T^*=0.1$ and $T^*=5$, the deviation is 6.7 and 7.5%, respectively.

B. Dependence on thermal history

To establish the dependence of the thermodynamic properties on the quench rate, we have investigated the temperature dependence of the thermodynamic properties at two higher cooling rates. The first, which we term our *instantaneous* quench, was performed by always starting at a same equilibrium configuration at $T^*=5$ and changing the temperature of the system at the very first time step to the final desired temperature in the range $T^*\in[0.1,1]$. The system was then allowed to equilibrate for 50τ and thermodynamic averages calculated over the next 150τ. For the second cooling program, which we call the *fast* quench, the starting configuration was the final configuration at $T^*=1$ from the instantaneous quench. The system was then cooled in steps of $\Delta T^*=0.1$ down to $T^*=0.1$, with an equilibration time of 50τ and a production run of 150τ at each step. In this cooling sequence, the initial configuration for each temperature step came from the final configuration of the directly preceding higher-temperature run.

The temperature dependence of U^* for both the fast and instantaneous quench are shown as asterisks and triangles, respectively, in Fig. 19, in comparison with our previous *slow* quench results that are listed in Table I and shown as circles in Fig. 19. We find that the higher the cooling rate, the earlier the departure of U^* from the equilibrium liquid line and the higher the glass transition temperature T_g^*, defined as the intersection temperature of the extrapolated liquid and glass lines. The glass transition region is also much broader for the instantaneous quench compared with the slow quench. Figure 19 also shows that the faster the cooling rate, the higher the potential energy of the quenched low-

temperature nonequilibrium states.

A number of workers [46,47] have suggested that the landscape of the potential energy surface over the configuration space has a ''top'' to it which is the average energy of the transition states between local minima. For temperatures above the characteristic temperature of this top, relaxation would occur without activation, while below this temperature dynamics becomes dominated by the local energy minima. One way of exploring this general attribute of the energy landscape is to study the outcomes of various quenches. Rapid quenches to $T^*=0.0$ from initial states prepared at $T^* \leqslant 0.3$ end up in low-energy states. (Interestingly, we find in these runs that the higher the initial temperature—in the range $T^* \leqslant 0.3$—the lower the resulting energy on quenching.) For $T^* \geqslant 0.4$, however, we find the system typically quenches into a relatively high energy minimum. This would suggest that the characteristic temperature of the landscape top (or, at least, an energy above a significant number of transition states) in the 2D mixture is $T^* \approx 0.35$.

C. Voronoi analysis of particle topologies

A discussion of the structure of a condensed phase involves separating the long-lived structural features from those transients associated with local oscillations. In the case of glassy states, we lack the simple broken symmetries which make the identification of the long-lived structure in crystals or hexatics so simple. The topology of particle positions provides an alternative reduced description of a configuration while still allowing amorphous arrangements to be characterized and differentiated from one another. Glaser and Clark [48] have presented a thoughtful discussion of the various ways such reduced descriptions can be obtained for a 2D liquid. We have used the Voronoi polygon construction [49] similar to that used by Deng *et al.* [3–6]. A Voronoi polygon associated with any particle contains all points closest to that particle than to any other particle. The edges of such a polygon are the perpendicular bisectors of the vectors joining the central particle to its nearest neighbors and the number of these edges is equal to the number of geometric neighbors for the associated particle. While the Voronoi construction provides a well defined algorithm for determining the topology of a given configuration, it does not necessarily accomplish as clean a separation of long-lived and transient structural fluctuations as we would wish. Specifically, a particle's coordination number as determined by its Voronoi polygon can sometimes undergo rapid changes due to thermal oscillations. Above $T^*=0$, then, we shall refer only to the general trends in coordination numbers.

We find that the average coordination number is 6 at all temperatures without fluctuation, suggesting that this is an exact value rather than a statistical one. [This is not the case if we use a cutoff distance taken from the first minimum of the total $g(r)$ to determine the number of nearest neighbors, where small fluctuations about six average first nearest neighbors are observed as shown in Figure 7(a).] Several explanations of why the average coordination number in 2D should be exactly 6 are provided in Refs. [49–51]. The assumptions on which these arguments are based are presented in the Appendix. Local coordination numbers other than 6

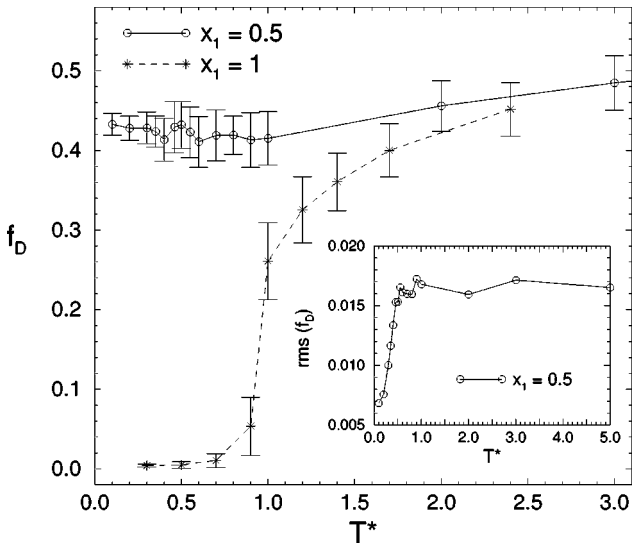

FIG. 20. The temperature dependence of the number fraction of defects f_D for the equimolar ($x_1=0.5$) binary mixture with $\sigma_2/\sigma_1=1.4$ and for the monocomponent system of small particles ($x_1=1$). The error bars are twice the standard deviation about the average data points. The results are averages over 1000 configurations during the production runs. The temperature dependence of the standard deviation (rms) of the defect fraction for the equimolar binary mixture is shown in the insert. Note the abrupt decrease in the amplitude of configurational fluctuations for $T^*<0.5$.

will be referred to as defects, although readers should note that this label is something of an anachronism, chosen so as to connect with ideas from single component systems only. As we shall see, these ''defects'' are an integral part of the stable amorphous ground states and should be regarded on equal footing with the hexagonal environments. Nearly all of the defects have coordination numbers of either 5 or 7, and, very infrequently, 4 or 8. At very low temperatures, all of the seven-coordinated particles are large and all of the five-coordinated ones are small.

The temperature dependence of the fraction of defects, $f_D=N_D/N$, where N_D is the total number of defects in the system, is plotted in Fig. 20 and compared with that for the single component system of small particles. For the pure liquid, f_D decreases substantially as the temperature drops below $T^*_{f,1}$ and has values close to zero in the crystalline solid at the very lowest temperatures. On the other hand, for the binary mixture, although there is a small decrease from $f_D=0.52$ at $T^*=5$ to $f_D=0.42$ at $T^*=1$, below $T^*=1 f_D$ remains approximately constant at $f_D \approx 0.43$. In contrast, Deng *et al.* [3,4] observe a significant reduction in the defect concentration on cooling in a mixture of Lennard-Jones discs with a diameter ratio of 1.244. Crystallization could be responsible for the decrease in this latter case since the diameter ratio is close to 1.2 for which it is not possible to prepare long-lived amorphous states in 2D.

While the average value of the number of defects show little variation with temperature for $T^* \leqslant 1$, the root mean square fluctuation $\sqrt{\langle f_D^2\rangle - \langle f_D\rangle^2}$, as shown in the inset in Fig. 20, exhibits a distinctive steplike increase as the temperature rises above $T^*=0.5$. This rather abrupt increase in fluctuations of the defect number coincides with similar features observed in the fluctuations of the enthalpy and vol-

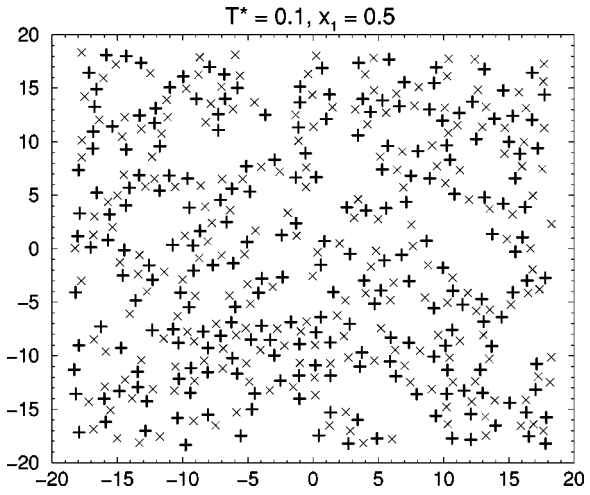

FIG. 21. The final configuration of the equimolar binary mixture ($\sigma_2/\sigma_1=1.4$) at $T^*=0.1$, showing only the positions of the particles which are not six-coordinated as determined by the Voronoi analysis described in Sec. V C. At this temperature, all of these defects consist of only five-coordinated small particles ($\times$) and seven-coordinated large particles ($+$).

ume. This connection will be explored in Sec. V E later below.

As already noted, the defects at low temperatures consist exclusively of equal numbers of sevenfold sites centered on large particles and fivefold sites centered on small particles. We find that these defects are strongly correlated spatially with every sevenfold defect adjacent to at least one fivefold defect for $T^*\leqslant 0.3$. Most of the sevenfold sites have two adjacent fivefold sites, a correlation which results in the dense network of defect chains throughout the sample, as shown in Fig. 21. The relationship between these correlations in the mixture and the melting models in 2D involving dislocation [52,53] or grain boundary [54] unbinding is taken up in Sec. V E.

D. Fluctuations and the associated material properties

The essential difference between the amorphous and the crystalline ground states lies in the very different kinds of low-temperature fluctuations each ground state supports. In this section we look at the fluctuations in enthalpy, volume, and stress in the amorphous mixture.

1. The heat capacity and related quantities

In the isothermal-isobaric ensemble, the constant pressure specific heat capacity $C_P=(\partial H/\partial T)_P$, the isothermal compressibility $\kappa_T=-V^{-1}(\partial V/\partial P)_T$, and the thermal expansion coefficient $\alpha_P=V^{-1}(\partial V/\partial T)_P$, can be calculated in reduced units from the following equations [55]:

$$C_P^*=\frac{C_P}{Nk_B}=\frac{N\langle \Delta H^{*^2}\rangle}{T^{*^2}}+1, \tag{26}$$

$$\kappa_T^*=\frac{\kappa_T\epsilon}{\sigma_1^2}=\frac{\langle \Delta V^{*^2}\rangle}{V^*T^*}, \tag{27}$$

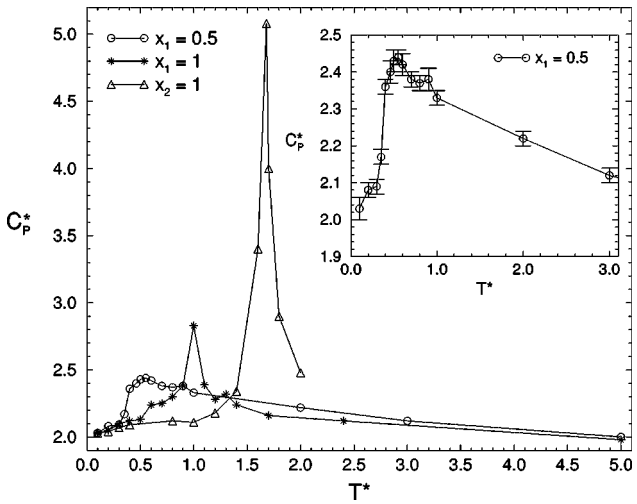

FIG. 22. The temperature dependence of the constant pressure specific heat capacity C_P^* for the equimolar binary mixture with $\sigma_2/\sigma_1=1.4$ ($\bigcirc$), and for the single component systems of small ($*$) and large ($\triangle$) particles. For the pure liquids, C_P^* diverges at the freezing points $T_{f,1}^*=0.95$ and $T_{f,2}^*=1.7$, respectively, as shown by the ''spikes'' in the figure where the data points just above and below the freezing transitions have been connected. The inset shows $C_P^*(T^*)$ for the binary mixture in more detail.

$$\alpha_P^*=\frac{\alpha_P\epsilon}{k_B}=\frac{N\langle \Delta V^*\Delta H^*\rangle}{V^*T^{*^2}}, \tag{28}$$

where $V^*=V\sigma_1^{-2}$ is the area (volume in 2D) in reduced units, and $\Delta H^*=H^*(t)-\langle H^*\rangle$ and $\Delta V^*=V^*(t)-\langle V^*\rangle$ are the fluctuations in the instantaneous enthalpy per particle and area respectively, with $\langle H^*\rangle$ and $\langle V^*\rangle$ being the averaged quantities. The angular brackets in the preceding equations denote an average over time. In Eq. (26), the constant 1 has to be added in order to correct for the lack of fluctuations in the kinetic energy due to the constant temperature constraint. In our MD simulations, the instantaneous thermodynamic properties were written out at regular short time intervals, enabling us to calculate the first order thermodynamic derivatives over a number of consecutive long time intervals. The results from the different time spans were then averaged and error estimates obtained.

The results for C_P^* are shown in Fig. 22 for the equimolar binary mixture (circles), as well as the monocomponent systems of small (asterisks) and large (triangles) particles. For the single component systems, C_P^* diverges at the freezing temperature, as shown by the ''spikes'' in Fig. 22. At the lowest temperatures we have studied, the reduced heat capacities per particle of the amorphous mixture equal those of the single component crystals, i.e., 2.0, the value expected for N classical harmonic oscillators in 2D. At high temperatures, the heat capacities of the mixture and single component mixtures again converge. Eventually, they must all reach the same ideal gas heat capacity per particle (2.0, in these units). It is in the temperatures between these limits that the supercooled mixture reveals the signature of its particular fluctuations.

For the binary mixture, the C_P^* curve, as shown in more detail in the inset of Fig. 22, consists of a highly asymmetric

peak with height ≈ 2.44 at $T^* = 0.55 \pm 0.05$, roughly the same temperature at which the α relaxation step first appears in the coherent and intermediate scattering functions. The abrupt decrease in the heat capacity below the peak temperature is generally attributed to the freezing out of modes as the system falls out of equilibrium. There is certainly clear evidence of failure to equilibrate for $T^* \leqslant 0.35$ (see Fig. 1). The decrease in C_P^* between $T^* = 0.55$ and 0.4, however, occurs at temperatures for which we believe that the amorphous mixture is properly equilibrated. We conclude that the peak is an equilibrium feature and that the temperature at which it occurs reflects a characteristic temperature $T^* \approx 0.35$ of the thermal fluctuations out of the amorphous ground state.

Can we identify the specific fluctuations which give rise to the main features of C_P^* for the mixture? While the details of the shape of the peak in C_P^* cannot be resolved, the sharp drop below $T^* = 0.5$ is substantial. We can resolve the fluctuations in the enthalpy H^* into the contributions due to potential energy fluctuations, volume fluctuations, and the cross term as follows:

$$C_p^* - 1 = \frac{N\langle \Delta H^{*2} \rangle}{T^{*2}} = \frac{N}{T^{*2}}\langle \Delta U^{*2} \rangle + \frac{2NP^*}{T^{*2}}\langle \Delta U^* \Delta V^* \rangle + \frac{NP^{*2}}{T^{*2}}\langle \Delta V^{*2} \rangle. \tag{29}$$

At $T^* = 0.5$, the contributions to C_P^* from the first, second, and third terms in the equation above are 0.030, 0.34, and 1.06, respectively. At all temperatures, the volume term is approximately 3 times greater than the cross term which in turn is one order of magnitude greater than the contribution from the fluctuations in the potential energy. The dominance of the component due to the volume fluctuations in the heat capacity peak is consistent with the importance of packing effects in this essentially steric model system. (It seems reasonable to speculate that the low-temperature heat capacity of weakly interacting particles, i.e., ''fragile'' liquids, will generally be dominated by density fluctuations.)

The step in C_P^* requires that there be some sort of enthalpy gap separating the ground state and the lowest ''excitation.'' The following simple model can account for this feature in a physically consistent fashion. With increasing thermal energy, the particle oscillations in the amorphous ground state will eventually develop anharmonic character. We shall assume that this anharmonicity occurs at localized regions and requires a configurational rearrangement involving a minimum volume increase. This minimal volume change δV arises from the discreteness inherent in packing and provides, in the form of the $P\delta V$ term, an ''excitation'' enthalpy. These excitations, by virtue of their anharmonic character, would be expected to contribute an enhanced expansivity. This is consistent with the jump in α_P^*, the thermal expansivity (see Fig. 23) which occurs at the same temperature as the jump in C_P^*. The absence of any such feature in the isothermal compressibility κ_T^*, also shown in Fig. 23, may reflect the relative insignificance of the local anharmonicities on the compressibility. One would expect this quantity to be governed, instead, by the load-bearing domains of high local rigidity. In our model of fluctuations, it is the additional volume change of the anharmonic regions which provides the sustained excess C_P^* at higher temperatures. The steady decrease with increasing temperature can be put down to the general decrease in the vibrational contribution with decreasing density. The increase in large amplitude motions associated with such anharmonicities would also account for the increase in the defect number fluctuations above $T^* = 0.5$ as shown in Fig. 20. The proposal that the discreteness inherent in dense random packings can give rise to an ''enthalpy gap'' in a classical system warrants further study.

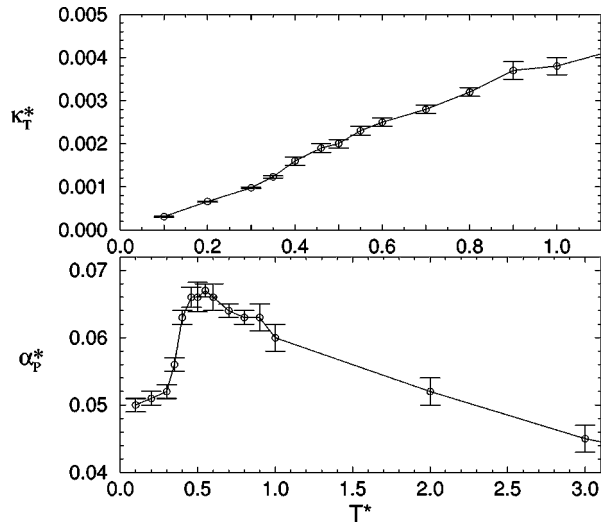

FIG. 23. The temperature dependences of the isothermal compressibility κ_T^* and the thermal expansion coefficient α_P^* for the equimolar binary mixture with $\sigma_2/\sigma_1 = 1.4$.

It is interesting to reflect on what ''heat capacity'' means in the unequilibrated glassy states for which relaxation is no longer observed. The heat capacity at constant pressure can be defined in two ways: in terms of the enthalpy fluctuations as in Eq. (26), and as the temperature derivative of the average enthalpy. In a system at equilibrium the two definitions are equivalent but what happens in the glassy states? We have compared the two formulas for C_P^* calculated over the entire temperature range studied. Due to the finite number of data points, we are not able to accurately calculate the derivative $d\langle H^* \rangle / dT^*$ at a given temperature, but we can estimate this quantity by the finite difference slope $\Delta H^*/\Delta T^*$ within a small temperature interval about the temperature of interest. This approximate derivative of the enthalpy is compared with the value of the heat capacity from the fluctuation formula for a range of temperatures in Table II. The two estimates of C_P^* are found to agree quite well over all temperatures. The slope $\Delta H^*/\Delta T^*$ also passes through a maximum at $T^* \approx 0.55$, although the height of this peak is slightly higher than that calculated from Eq. (26). This unexpected persistence of equilibrium relationships into nonequilibrium states has also been noted by Evans *et al.* [56] in an interesting recent study of the configurational temperature. The simplest rationalization of this result is that both measures of C_p reflect the dynamically accessible space of enthalpy fluctuations and are dominated by the fastest fluctuations which remain equilibrated at all T^*.

TABLE II. The constant pressure specific heat capacity C_P^* for the 2D binary mixture at various temperatures calculated from (i) the slope of the average enthalpy over a temperature interval between T_1^* and T_2^* and (ii) the fluctuations in the enthalpy. The average enthalpy per particle H^* for a range of temperatures is given in Table I.

T^*	T_1^*	T_2^*	$C_P^*(T^*)=\frac{dH^*(T^*)}{dT^*}\approx\frac{H^*(T_1^*)-H^*(T_2^*)}{(T_1^*-T_2^*)}$	$C_P^*(T^*)=\frac{N\langle\Delta H^{*2}\rangle}{T^{*2}}+1$
3	2	5	2.12	2.12
1	0.9	2	2.30	2.33
0.7	0.6	0.8	2.41	2.38
0.6	0.55	0.7	2.43	2.42
0.55	0.5	0.6	2.53	2.44
0.5	0.46	0.55	2.51	2.43
0.4	0.35	0.46	2.44	2.36
0.35	0.3	0.4	2.16	2.17
0.2	0.1	0.3	2.07	2.08

2. The high frequency shear modulus and stress fluctuations

In what ways do an amorphous ground state differ from a crystalline one on a *local* level? Discussion of the absence of global order in the former, for example, is irrelevant here. It is the differences in local properties that can be directly related to differences in particle mobility on heating. One significant difference in the two types of stable ground state is the distribution of local stress. The contribution of particle i in a single configuration to the component $\sigma_{\alpha\beta}$ of the stress tensor ($\alpha\beta$ standing for xx, yy, or xy) can be calculated as follows [57]:

$$\sigma_{\alpha\beta}(i)=\frac{1}{V}\left(\frac{p_{i\alpha}p_{i\beta}}{m_i}+\frac{1}{2}\sum_{j\neq i}^{N}\mathbf{r}_{ij\alpha}F_{ij\beta}\right),\quad \alpha,\ \beta=x \text{ or } y, \tag{30}$$

where m_i is the atomic mass of particle i, $p_{i\alpha}$, and $p_{i\beta}$ are the α and β components of the momentum of particle i, $\mathbf{r}_{ij\alpha}$ is the α component of the vector joining particles i and j, $F_{ij\beta}$ is the β component of the force exerted on particle i by particle j, and V is the volume of the system. Note that in a 2D system, $\sigma_{xy}=\sigma_{yx}$.

In Fig. 24, we present the distribution of contributions per particle to the reduced shear stress $\sigma_{xy}^*(=\sigma_{xy}\sigma_1^2/\epsilon)$ of an amorphous mixture and a single component crystal, both at zero temperature. Note the substantial increase in the distribution width of shear stress in the amorphous ground state over that of the crystal. The distributions of local compression $(\sigma_{xx}^*+\sigma_{yy}^*)/2$ for the two different systems are presented in Fig. 25. Again the difference in width of the distributions is substantial. Our observations concerning the stress heterogeneities of the glassy configurations are as follows. (1) The stress distribution is very broad. Results from simulations of metallic alloys [58] and fused silica [59] indicate that a substantial number of atoms can be under shear stress which exceeds the yield stress of the material. We have not yet established the yield stress of the amorphous 2D mixture. (2) While the width of the stress distributions decreases somewhat with lower cooling rates, the heterogeneity is an unavoidable consequence of the disorder. The stress distribution, in other words, is an inherent property of the amorphous ground state which cannot be ''annealed'' out except by crystallization. (3) The sites of high compression, σ_{xx}^* and σ_{yy}^*, tend to form extended ''backbones'' along the x and y directions, respectively. High shear stress, on the other hand, is distributed in local pockets without any obvious correlation. (4) We have been unable to find any correlation between local relaxation times and local stress. Deng *et al.* [5] have observed similar stress heterogeneity in a 2D mixture, along with spatial fluctuations in volume and enthalpy. These authors provide an interesting discussion of the role of these fluctuations in the response of the 2D glass to a shear strain [6].

The infinite frequency shear modulus G_∞ is related to the fluctuating shear stress by

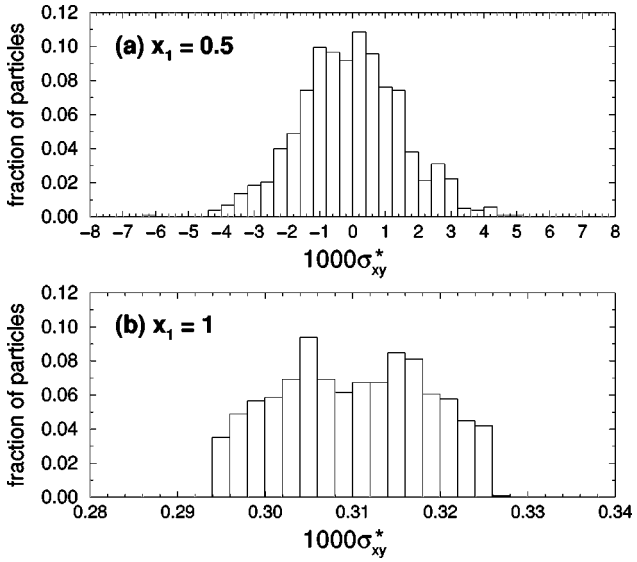

FIG. 24. The distribution of local shear stress σ_{xy}^*, as defined in Eq. (30), for states of the (a) equimolar binary mixture and (b) the single component crystal of small particles at $T^*=0$. For the binary mixture, the state at $T^*=0$ was obtained by quenching the final configuration of the slow run at $T^*=0.1$. The vertical axes denote the fraction of particles with local shear stress lying between $\sigma_{xy}^*-\Delta/2\leq\sigma_{xy}^*(i)<\sigma_{xy}^*+\Delta/2$. Observe, from the difference in the scales of the horizontal axes, that the width of the distribution is much broader in the amorphous state compared to the pure crystal.

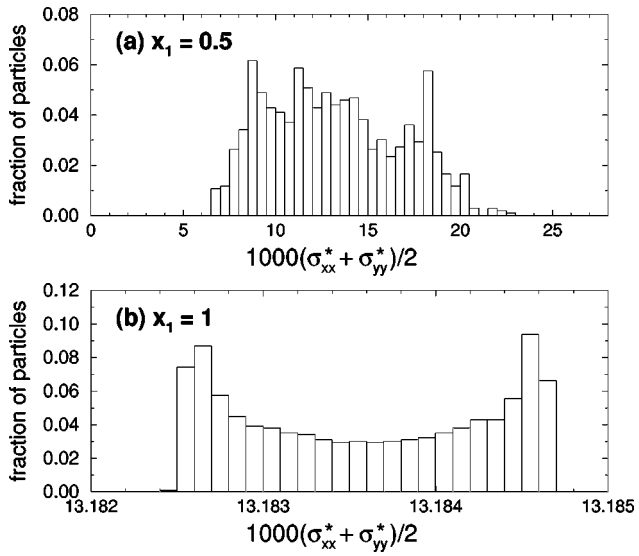

FIG. 25. The distribution of the local compression $(\sigma^*_{xx}+\sigma^*_{yy})/2$ for the amorphous binary mixture and the pure crystalline state at $T^*=0$. Again observe the difference in the horizontal scales.

$$G_\infty=\frac{V}{k_BT}\langle\sigma_{xy}(0)\sigma_{xy}(0)\rangle,$$

where

$$\sigma_{xy}(0)=\sum_{i=1}^{N}\sigma_{xy}(i) \quad \text{at } t=0. \tag{31}$$

In the case of a harmonic solid $G_\infty=E$, where E is the shear modulus. The temperature dependence of $G^*_\infty=G_\infty\sigma_1^2/\epsilon$ is shown in Fig. 26. Note its constancy down to $T^*=0.4$ in contrast to the increase in relaxation time of more than 3 orders of magnitude over that same temperature interval (see Fig. 2). The rapid rise in the modulus at the lowest temperatures is puzzling, given that there is little change in density

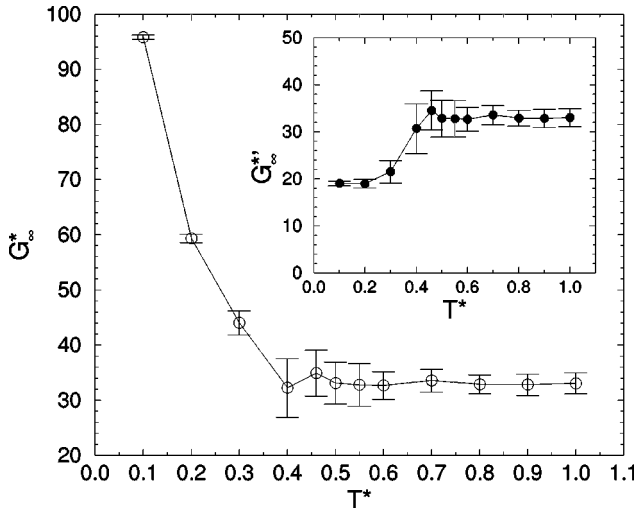

FIG. 26. The infinite frequency shear modulus G^*_∞, calculated using Eq. (31), for the equimolar mixture over $0.1\leqslant T^*\leqslant 1.0$. The insert shows the temperature dependence of the shear modulus minus the contribution from the mean shear stress as discussed in the text.

or structure over this temperature interval which could account for the large increase. In fact, this increase is an artifact, arising from the assumption in Eq. (31) that the mean shear stress is zero. While always true for the equilibrium liquid, this condition breaks down once relaxation is too slow to permit equilibration. The true shear modulus, corrected for the frozen-in stress, $G^{*\prime}_\infty=G^*_\infty-V^*\langle\sigma^*_{xy}(0)\rangle^2/T^*$, is plotted in the inset of Fig. 26. Now we find the large increase in the shear modulus at low temperatures has been replaced by a decrease. Dyre *et al.* [60] have proposed that the non-Arrhenius temperature dependence of relaxation in a supercooled liquid arises from the temperature dependent increase in the infinite frequency shear modulus upon cooling. In the case of the 2D mixture, we find a non-Arrhenius temperature dependence for the relaxation time (Fig. 2) without any such increase in $G^{*\prime}_\infty$.

E. Approaching the ground state: Phase transition or continuous arrest?

Do the elementary fluctuations of the amorphous ground state described in relation to C_P interact sufficiently with one another to result in a phase transition between an amorphous ground state and the relaxing liquid? There is, of course, a considerable history of speculation concerning such a transition [61]. In this section we consider how the mixture leaves the ground state on heating and the connection between this picture and those associated with various transition models.

The possible thermodynamic transitions can be broadly differentiated in terms of what is regarded as the elementary fluctuation: an ordered cluster or a structural defect. The model of glass formation presented in Ref. [9] involves the former choice. Here, structural arrest is assumed to be the result of the instability (or near instability) of the liquid with respect to crystal formation. The amorphous ground state is a fused and kinetically frustrated mass of crystalline nuclei. (Other cluster models have been proposed which are considerably less explicit about the order parameters which define the cluster [30] and therefore less available for direct testing.) In Sec. III B 2 we noted the absence of any accessible spinodal in the 2D mixture and, in the following section, demonstrated the absence of extended orientational correlations in the low-temperature amorphous phase. This latter observation does not necessarily preclude the existence of a cluster made up of orientationally *uncorrelated* hexagonal domains [9]. Elsewhere [2] we have found only a weak correlation between local relaxation time and local degree of hexagonal order. This bears out the general observation that hexagonal arrangements do not necessarily correspond to the most stable structure in a well dispersed mixture. While the spinodal model quite rightly places emphasis on the role of stable packings, it neglects the possibility of rigidity arising from configurations other than crystalline. The observation of an extended and dense network of nonhexagonal environments, as shown in Fig. 21, points to rigidity appearing as a property of an entire configuration, not just clusters of hexagonal sites.

The alternative picture is to start with the rigid amorphous ground state and consider the fluctuations responsible for the heat capacity peak and, ultimately, structural relaxation. The dislocation-unbinding transition of Kosterlitz and Thouless (KT) [52] provides a well analyzed model of a transition

involving elementary structural fluctuations (defects) about a 2D ground state (hexagonal crystal). Following our discussion in Sec. V D 1, the role of defect is played by a local structural fluctuation associated with the appearance of anharmonic response. Whatever form this defect takes, it is unlikely to meet the key requirements of defects for the KT transition. In the case of the single component crystal, dislocation energy depends logarithmically on the system size due to long-range strain fields. These defects interact via these stain fields as well as through the renormalization of the elastic moduli. The high density of grain boundaries in the equimolar binary mixture would be expected to screen any strain field of the proposed anharmonic fluctuations, resulting in defect energies mainly due to the core rather than the extended field. (For small diameter ratios, such as that used in Ref. [3], a smaller defect density is possible. In such cases, the asymptotic interaction may play an important role.) The core energy depends on the local packing efficiency rather than the effective elastic modulus. This would seem to rule out a collective transition of the KT kind.

What is known about the transitions of disordered systems in 2D is based entirely on the action of applied disordering fields. It is standard to suggest that slowly relaxing degrees of freedom be treated as the source of a disordered field. While this approximation may shed some light on the response of the faster degrees of freedom, they can tell us little about the origin of the slow degrees of freedom themselves. Nelson [25] has examined the role of long wavelength disorder, noting that it lowers the melting point with increasing amplitude of the disorder until, above a critical value of this parameter, translational order is no longer possible. This earlier work leaves unanswered the description of the low-temperature state above this critical disorder. More recently, it has been established [63,64] that an elastic solid undergoes a pinning transition in the presence of a disordered potential on cooling below some temperature T_g. This transition, however, vanishes if the particles are permitted to relax their topological connectivity [63]. Inclusion of thermal dislocations and pinning disorder [65] appears to produce a ''glassy regime'' in which the liquid 'freezes' into a state without long-range order. This transition also appears to vanish at high pinning strengths, again leaving the nature of the low-temperature disordered state above this critical pinning strength unspecified. While it remains to be seen what relevance, if any, these models have for the amorphous binary mixture, they do appear to provide an example of a transition between two disordered phases.

One difficulty in the application of these pinning models to the 2D mixture is in the manner in which disorder is introduced. The mixture case would seem to be better described by inclusion of a fixed concentration of local defects rather than an external field with long wavelength correlations. The KT theory assumes that the energy of an isolated dislocation (the ''core'' energy) is large so that the transition is dominated by the unbinding of a relatively small number of defects. Saito [62], following up on a proposal by Chui [54], examined the consequences of a small core energy. Given the high concentration of inherent ''defects'' in the amorphous mixture, the binary system is closer to Saito's small core energy scenario. In the case of thermally excited defects, this condition results in a first order transition, via a mechanism similar to the grain boundary unbinding transition proposed by Chui. The story is different in the equimolar mixture for two reasons. First, the grain boundaries are already dense at $T^*=0$ so, while there may be a transition from pinned to mobile boundaries, there is no significant change in structure. Second, the defects are stabilized by local packing effects that owe little to the asymptotic elastic interaction used in previous defect models (see the Appendix). While this short-range interaction differs significantly from the long-range form typically assumed, we note that at the high density of defects in the equimolar mixture, this difference may not be significant. If the picture of a pinning transition for nonthermal grain boundaries seems to be progress, it should not. The ''pinning'' is self-imposed (not the result of a fixed external field) and so is essentially the same problem as that of describing the self-arrest of particle motions which we began with. What is more, this picture is based on the assumption that the topological defects identified in Sec. V C are also the sites of the anharmonic excitations, i.e., that the mobility occurs at a defect line. The equivalent notion that hexagonal order denotes stability simply is not correct in the binary mixture where, for example, sixfold coordination of a large particle by small particles is a quite ''loose'' configuration. Progress along this line of thinking will depend on establishing a clearer structural picture of the important anharmonic fluctuations.

VI. CONCLUSION

In this paper we have presented a study of the structural and thermodynamic properties of a simulated supercooled 2D binary mixture. The mixture exhibits a metastable amorphous phase with a relaxation time that increases rapidly with decreasing temperature in the absence of any long-range structural correlations. These results, taken with the dynamics of this same system [2], establish the simulated 2D mixture as a member of the class of fragile glass formers which includes orthoterphenyl and salol. While questions may remain concerning the relevance of either 2D or simulated models in general to the origin of slow dynamics in other specific glass-forming liquids, there is no question that this model exhibits the full range of glass phenomenology and does so in a physically consistent fashion.

Here is a summary of the main results of this study.

(1) The equimolar binary mixture shows no evidence of long-range order, either translational or orientational, over the entire temperature range studied. The average local hexagonal order increases continuously from the equilibrium liquid to the arrested solid. Our results indicate considerable continuity between liquid and glass.

(2) The phase diagram for the binary mixture with diameter ratio of 1.4 has been calculated via thermodynamic integration with the assumption of immiscibility in both ordered crystals. The most striking feature of this phase diagram is the deep eutectic point at $x_1=0.75$ and $T^*=0.54$. This depression of the coexistence temperature is quite substantial compared to the freezing temperatures $T^*_{f,1}=0.95$ and $T^*_{f,2}=1.7$ of the single component system of small ($x_1=1$) and large particles, respectively. The presence of a deep eutectic in a system with only repulsive interactions indicates that a significant mismatch in particle sizes is sufficient to substantially depress the freezing transition

without the need for large attractive interactions between unlike particles. The stability of the metastable liquid is underscored by the presence of substantial local crystalline fluctuations.

(3) Below $T^* \approx 0.5$, the enthalpy and density were found to increase with increasing quench rate while above this temperature, variation of the quench rate had little effect. This is consistent with a rapid increase in relaxation times below $T^* = 0.5$. An alternative measure of the ''top'' of the energy landscape, involving the minimum initial temperature necessary to quench into high-energy minima, resulted in a characteristic temperature of $T^* \approx 0.35$. These two values might be accounted for as reflecting the maximum and minimum transition state energies, respectively.

(4) Local topological ''defects,'' in the form of nonhexagonal environments, are found to obey a number of nontrivial constraints. These are (i) the equality in numbers of fivefold and sevenfold sites, (ii) the near constancy of the number of defects over the entire temperature range, and (iii) the perfect ''binding'' of fivefold and sevenfold sites (i.e., each fivefold site has at least one sevenfold neighbor and vice versa) as the temperature approaches zero. The mean squared deviation in the number of defects was found to increase abruptly at $T^* \approx 0.35$, coinciding with a similar abrupt increase in C_P^*.

(5) The zero-temperature configurations (referred to here as the ground state) exhibited a broad distribution of local shear and compressional stress as compared to that found in the single component crystal. It was argued that this inherent stress heterogeneity is an unavoidable feature of the amorphous ground state, differentiating it qualitatively from the crystal configuration. The mechanical and chemical consequences of this stress heterogeneity remain unexplored [59]. The high frequency shear modulus was found to be temperature independent in the range $0.4 \leqslant T^* \leqslant 1.0$. The apparent increase below $T^* = 0.4$ is a consequence of a nonzero shear stress average, a consequence of structural arrest on the simulation time scale.

(6) The heat capacity at constant pressure of the mixture exhibits a highly asymmetric peak, similar in shape and magnitude to C_P for fragile liquids. The heat capacity undergoes a rapid rise with increasing temperature at $T^* \approx 0.35$, achieving a maximum value of 2.44 at $T^* = 0.55$ and then gradually decreasing, roughly linearly with temperature, all the way up to the highest temperatures studied. The continued satisfaction of the equilibrium relationship between fluctuations and derivatives in demonstrably unequilibrated liquids was demonstrated. It is argued that this is a result of the separation of times scale which ensures that those modes which are kinetically able to participate as fluctuations at all are fast enough to also be equilibrated.

(7) While the low value of C_p^* below $T^* = 0.4$ certainly includes the accepted nonequilibrium effect of ''freezing out'' of configurational degrees of freedom, we argue that the initial drop in the heat capacity for $0.4 \leqslant T^* \leqslant 0.55$ takes place in equilibrated samples. This implies the presence of an ''enthalpy gap'' with a characteristic temperature of $T^* \approx 0.35$. It is proposed that this gap corresponds to the minimum volume increase required to allow a local configuration access to anharmonic motion. The fact that this minimal volume change is not zero is a consequence of the discreteness of particle packing. The abrupt increase in C_P^* is attributed to the increase in configurational fluctuations associated with these larger amplitude motions. This also accounts for the increase in fluctuations in defect number. The sustained excess heat capacity at high temperatures is the result of the increased expansivity (due to the anharmonic excitations) which provides for enhanced density fluctuations over that possible in the crystal.

The reduced dimensionality and its associated reduction in the space of fluctuations holds out the possibility of developing a satisfactory conceptual picture of the statistical correlations in this particular glass-forming liquid. This picture must address the two basic issues concerning the static properties of a supercooled liquid: the structure and stability of the ground states, and the nature of the thermal fluctuations that first take us beyond harmonic fluctuations about such ground states. The progress made in assembling this picture is outlined above. Here, we need to note the shortfalls. We remain unable to identify any general structural criteria associated with amorphous ground states. While pictures of crystalline clusters or pinned grain boundaries provide reassuring rationalizations for structural arrest, their significance can only be understood within the framework provided by these unknown criteria for stability and, hence, rigidity. It also remains unclear whether the anharmonic excitations identified in this paper are associated with particular types of local structure and, if so, what is the structural signature of these ''soft'' spots?

This difficulty in establishing the structural features relevant to glass formation provides the motive for the study of dynamic heterogeneities in recent years [2,8,17,66–70]. In the absence of any substantial changes in structure on supercooling, we are left with only the changes in dynamics, both the dramatic and the subtle, to provide the clues as to the character of the underlying stability. Kinetic inhomogeneities currently provide the only sure means of characterizing the fluctuations involved in slow relaxation in the glass formers. In this sense the glass transition invites an inversion of the normal conceptual approach in condensed matter problems. Instead of proceeding from structure to dynamics, we go from dynamics to structure. The goal, of course, remains the same; to establish the functional connection between the two.

ACKNOWLEDGMENTS

We gratefully acknowledge the contribution of Bronwyn Elliott to the analysis presented in the Appendix. We would also like to thank Austen Angell for valuable discussions concerning heat capacities, and the Supercomputer Facility at the Australian National University for generous grants of computer time. One of us (D.N.P.) would like to thank the Japanese government for financial support from the Science and Technology Agency.

APPENDIX

Here we present some discussion of two aspects of packing in a binary mixture of hard discs relating to the number and correlation of the defects as described in Sec. V C.

1. Why is the average number of neighbors 6?

While this question has been discussed already in the literature [49–51], important assumptions are sometimes left

unstated. A configuration of discs can be reduced to a tiling of the plane using the following procedure. First, the neighbors of each particle are established via a Voronoi construction as described in Sec. V C. Next, the centers of neighboring particles are joined by straight lines (a Delaunay construction). Each particle now replaced by a vertex of these lines or *edges*. The area enclosed by a set of edges is a *face*. The argument that the average number of edges per vertex is 6 goes as follows. The key assumption is that the faces are all triangular. This is the same as assuming that every pair of neighbors of a particle that are adjacent to one another are also neighbors of one another (i.e., joined by an edge). We are unaware of a proof of this proposal.

A relation, due to Euler [71], exists between the number of vertices V, faces F, and edges E,

$$V-E+F=2. \tag{A1}$$

Perhaps the easiest proof of this result can be found in Ref. [71] in which it is shown that for a connected graph of edges and vertices the quantity $V-E+F$ is unchanged when an edge is removed along with associated vertices necessary to ensure the new graph is also connected. Eventually one runs out of edges (i.e., $E=0$) and is left with a single face and a single vertex (this is ensured by the connectivity condition) so that $V-E+F=2$.

The assumption of only triangular faces implies that

$$2E=3F. \tag{A2}$$

Substituting this result into Euler's relation gives

$$3V=E+6. \tag{A3}$$

As V (equal to the number of particles) goes to infinity (and, acknowledging that in this limit each edge contributes to the valency of two vertices), we find that the average number of edges per vertex is 6, as observed.

2. What is the origin of the strong sevenfold-fivefold pairing observed in the amorphous ground state?

The most likely alternative to sevenfold-fivefold pairing would be to have the seven neighbors of a large particle all finding themselves in sixfold sites. To explore the likelihood of this situation consider a large particle surrounded by only small particles. It is possible to arrange seven small hard discs (the first shell) about a large one so that each of the small discs is, in turn, surrounded by six discs. The arrangement involves a high degree of heptagonal symmetry in both the first, second, and third shells of small particles (as shown in Fig. 27). Perturb this symmetry and the probability of finding a fivefold site among the 1st shell particles quickly rises. For example, if we push a third shell particle into contact with a first shell particle while maintaining as regular a packing as possible elsewhere we find roughly 76% of the configurations (as counted by generating the topologically distinct graphs arising due to this perturbation) include a fivefold site about one of the members of the first shell.

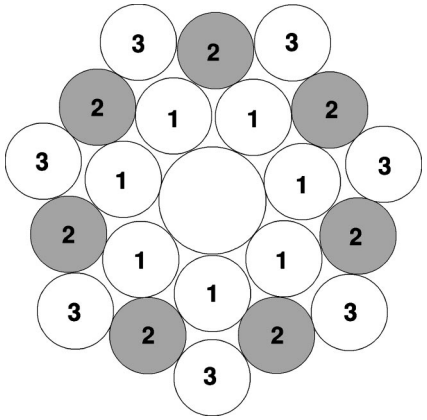

FIG. 27. Packing of hard discs about a large disc indicating the first, second, and third solvation shells as discussed in the Appendix.

Now add one large particle to either the first, second, or third shell. It is still possible to pack the discs such that all of the first shell particles are sixfold coordinated. Add a second large particle to the second shell. If it is in contact with the other ''solvating'' large disc then there will be a fivefold site among the first shell particles. Assuming an equimolar mixture and neglecting compositional correlation, the probability of there *not* being two large particles in contact in the three solvation shells (one of the large particles being in the second shell) is 0.17. Factoring in the possibility of irregular packings as considered above and the probability of there *not* being at least one fivefold site among the seven discs surrounding the central large particle drops to only 0.004. Averaging over the possible compositions of the three solvation shells and we find the sevenfold-fivefold pairing becomes effectively unavoidable under close-packing conditions.

[1] P. W. Anderson, *Basic Notions of Condensed Matter Physics* (Frontiers in Physics Lecture Series, Benjamin Publishing, 1984).
[2] D. N. Perera and P. Harrowell (unpublished).
[3] D. Deng, A. S. Argon, and S. Yip, Philos. Trans. R. Soc. London, Ser. A **329**, 549 (1989).
[4] D. Deng, A. S. Argon, and S. Yip, Philos. Trans. R. Soc. London, Ser. A **329**, 575 (1989).
[5] D. Deng, A. S. Argon, and S. Yip, Philos. Trans. R. Soc. London, Ser. A **329**, 595 (1989).
[6] D. Deng, A. S. Argon, and S. Yip, Philos. Trans. R. Soc. London, Ser. A **329**, 613 (1989).
[7] T. Muranaka and Y. Hiwatari, Phys. Rev. E **51**, R2735 (1995).
[8] R. Yamamoto and A. Onuki, J. Phys. Soc. Jpn. **66**, 2545 (1997); Europhys. Lett. **40**, 61 (1997); Phys. Rev. E **58**, 3515 (1998).
[9] A. I. Mel'cuk, R. A. Ramos, H. Gould, W. Klein, and R. D. Mountain, Phys. Rev. Lett. **75**, 2522 (1995).
[10] M. R. Sadr-Lahijany, P. Ray, and H. E. Stanley, Phys. Rev. Lett. **79**, 3206 (1997).
[11] L. Bocquet, J. P. Hansen, T. Biben, and P. Madden, J. Phys.: Condens. Matter **4**, 2375 (1992).
[12] R. B. Schwarz and W. L. Johnson, Phys. Rev. Lett. **51**, 415 (1983).

[13] D. J. Evans and G. P. Morriss, Chem. Phys. **77**, 63 (1983); Comput. Phys. Rep. **1**, 297 (1984).
[14] M. P. Allen and D. J. Tildesley, *Computer Simulations of Liquids* (Oxford University Press, Oxford, 1987).
[15] D. N. Perera and P. Harrowell, Phys. Rev. Lett. **81**, 120 (1998).
[16] D. N. Perera and P. Harrowell, J. Non-Cryst. Solids **235-237**, 314 (1998).
[17] M. M. Hurley and P. Harrowell, Phys. Rev. E **52**, 1694 (1995).
[18] D. N. Perera, Ph.D. thesis, University of Sydney, Australia, 1998 (unpublished).
[19] B. Bernu, J. P. Hansen, Y. Hiwatari, and G. Pastore, Phys. Rev. A **36**, 4891 (1987).
[20] W. Kob and H. C. Andersen, Phys. Rev. E **51**, 4626 (1995).
[21] J. P. Hansen and I. R. McDonald, *Theory of Simple Liquids* (Academic Press, London, 1976), p. 97.
[22] M. P. Allen and D. J. Tildesley, *Computer Simulations of Liquids* (Ref. [14]), pp. 338–339.
[23] C. Unger and W. Klein, Phys. Rev. B **29**, 2698 (1984); W. Klein and F. Leyvraz, Phys. Rev. Lett. **57**, 2845 (1986).
[24] K. Bagchi, H. C. Andersen, and W. Swope, Phys. Rev. Lett. **76**, 255 (1996); Phys. Rev. E **53**, 3794 (1996).
[25] D. R. Nelson, Phys. Rev. B **273**, 2902 (1983).
[26] J. Q. Broughton, G. H. Gilmer, and J. D. Weeks, J. Chem. Phys. **75**, 5128 (1981).
[27] J. Q. Broughton, G. H. Gilmer, and J. D. Weeks, Phys. Rev. B **25**, 4651 (1982).
[28] W. G. Hoover, S. G. Gray, and K. W. Johnson, J. Chem. Phys. **55**, 1128 (1971).
[29] Y. Hiwatari, H. Matsuda, T. Ogawa, N. Ogita, and A. Ueda, Prog. Theor. Phys. **52**, 1105 (1974).
[30] S. A. Kivelson, X. Zhao, D. Kivelson, T. M. Fischer, and C. M. Knobler, J. Chem. Phys. **101**, 2391 (1994).
[31] H. Xu and M. Baus, J. Phys.: Condens. Matter **2**, 5885 (1990).
[32] R. J. Wheatley, Mol. Phys. **93**, 965 (1998).
[33] W. G. T. Kranendonk and D. Frenkel, Mol. Phys. **72**, 679 (1991); **72**, 699 (1991); **72**, 715 (1991).
[34] H. Miyagawa and Y. Hiwatari, Phys. Rev. A **40**, 6007 (1989).
[35] J.-L. Barrat, J.-N. Roux, and J.-P. Hansen, Chem. Phys. **149**, 197 (1990).
[36] A. R. Denton and N. W. Ashcroft, Phys. Rev. A **42**, 7312 (1990).
[37] R. J. Speedy and R. K. Bowles, J. Chem. Phys. **110**, 4559 (1999).
[38] *Binary Alloy Phase Diagrams*, edited by T. B. Massalki, J. L. Murray, L. H. Bennett, and H. Baker (ASM, Ohio, 1987), Vol. 1, p. 313 (Au-Si), p. 492 (Cd-Bi), Vol. 2, p. 1245 (Ge-Sb), p. 1265 (Ge-Zn), p. 1739 (Ni-P). The eutectic depth for the Ni-P system is measured relative to the melting point of the Ni_3P compound, since the eutectic point lies between the pure metal and this compound.
[39] H. S. Chen and D. Turnbull, J. Appl. Phys. **38**, 3646 (1967).
[40] J. J. Gilman, Philos. Mag. B **37**, 577 (1978).
[41] H. S. Chen, Rep. Prog. Phys. **43**, 353 (1980).
[42] T. A. Weber and F. H. Stillinger, Phys. Rev. B **31**, 1954 (1985).
[43] P. W. Atkins, *Physical Chemistry*, 3rd ed. (Oxford University Press, Oxford, 1988), p. 173.
[44] D. N. Perera and P. Harrowell, Phys. Rev. Lett. **80**, 4446 (1998).
[45] R. J. Speedy, Mol. Phys. **95**, 169 (1998).
[46] H. Jonsson and H. C. Andersen, Phys. Rev. Lett. **60**, 2295 (1988).
[47] S. Sastry, P. G. Debenedetti, and F. H. Stillinger, Nature (London) **393**, 554 (1998).
[48] M. A. Glaser and N. A. Clark, Adv. Chem. Phys. **88**, 543 (1993).
[49] R. Collins, in *Phase Transitions and Critical Phenomena*, edited by C. Domb and M. S. Green (Academic, London, 1972), Vol. 2, p. 271.
[50] J. P. McTague, D. Frenkel, and M. P. Allen, in *Ordering in Two Dimensions*, edited by S. K. Sinha (Elsevier North-Holland, New York, 1980), pp. 147–153.
[51] T. A. Weber and F. H. Stillinger, J. Chem. Phys. **74**, 4020 (1981).
[52] J. M. Kosterlitz and D. J. Thouless, J. Phys. C **6**, 1181 (1973); J. M. Kosterlitz, *ibid.* **7**, 1046 (1974).
[53] B. I. Halperin and D. R. Nelson, Phys. Rev. Lett. **41**, 121 (1978); D. R. Nelson and B. I. Halperin, Phys. Rev. B **19**, 2457 (1979).
[54] S. T. Chui, Phys. Rev. Lett. **48**, 933 (1982).
[55] M. P. Allen and D. J. Tildesley, *Computer Simulations of Liquids* (Ref. [14]), pp. 51–54.
[56] B. D. Butler, G. Ayton, O. G. Jepps, and D. J. Evans, J. Chem. Phys. **109**, 6519 (1998).
[57] M. P. Allen and D. J. Tildesley, *Computer Simulations of Liquids* (Ref. [14]), p. 60.
[58] T. Egami and V. Vitek, J. Non-Cryst. Solids **61-62**, 499 (1984); S. Chen, T. Egami, and V. Vitek, *ibid.* **75**, 449 (1985); T. Egami and V. Vitek, Mater. Res. Soc. Symp. Proc. **57**, 199 (1987); V. Vitek and T. Egami, Phys. Status Solidi B **144**, 145 (1987); D. T. Kulp, T. Egami, D. E. Luzzi, and V. Vitek, J. Non-Cryst. Solids **156**, 510 (1993); J. Alloys Compd. **194**, 417 (1993).
[59] B. Elliott and P. Harrowell (unpublished).
[60] J. C. Dyre, N. B. Olsen, and T. Christensen, Phys. Rev. B **53**, 2171 (1996); N. B. Olsen, J. C. Dyre, and T. Christensen, Phys. Rev. Lett. **81**, 1031 (1998).
[61] J. Jäckle, Rep. Prog. Phys. **49**, 171 (1986).
[62] Y. Saito, Phys. Rev. B **26**, 6239 (1982).
[63] C. Carraro and D. R. Nelson, Phys. Rev. E **56**, 797 (1997).
[64] D. Carpentier and P. Le Doussal, Phys. Rev. B **55**, 12 128 (1997).
[65] D. Carpentier and P. Le Doussal, Phys. Rev. Lett. **81**, 1881 (1998).
[66] C. Donati, J. F. Douglas, W. Kob, S. J. Plimpton, P. H. Poole, and S. C. Glotzer, Phys. Rev. Lett. **80**, 2338 (1998); **79**, 2827 (1997).
[67] S. Butler and P. Harrowell, J. Chem. Phys. **95**, 4454 (1991); **95**, 4466 (1991).
[68] P. Harrowell, Phys. Rev. E **48**, 4359 (1993).
[69] M. Foley and P. Harrowell, J. Chem. Phys. **98**, 5069 (1993).
[70] M. M. Hurley and P. Harrowell, J. Chem. Phys. **105**, 10 521 (1996); **107**, 8586 (1997).
[71] O. Ore, *Graphs and Their Uses*, revised and updated by R. J. Wilson (The Mathematical Association of America, Washington, 1990), p. 114; D. Barnette, *Map Coloring, Polyhedra and the Four Color Problem*, Vol. 8 of *The Dolciani Mathematical Expositions* (Mathematical Association of America, 1983); see also B. Grünbaum and G. C. Shepard, *Tilings and Patterns* (W. H. Freeman, New York, 1987).